

1 **A Genome-Wide Association Analysis Reveals a Role for Recombination in the Evolution  
2 of Antimicrobial Resistance in *Burkholderia multivorans***

3  
4 Julio Diaz Caballero<sup>1</sup>, Shawn T. Clark<sup>2,3</sup>, Pauline W. Wang<sup>4</sup>, Sylva L. Donaldson<sup>4</sup>, Bryan  
5 Coburn<sup>5</sup>, D. Elizabeth Tullis<sup>6</sup>, Yvonne C.W. Yau<sup>3,7</sup>, Valerie J. Waters<sup>8</sup>, David M. Hwang<sup>2,3,9</sup>,  
6 David S. Guttman<sup>1,4,\*</sup>

7  
8 <sup>1</sup>Department of Cell and Systems Biology, University of Toronto, Toronto, Ontario, Canada  
9 <sup>2</sup>Latner Thoracic Surgery Laboratories, University Health Network, University of Toronto,  
10 Toronto, Ontario, Canada

11 <sup>3</sup>Department of Laboratory Medicine and Pathobiology, University of Toronto, Toronto, Ontario,  
12 Canada

13 <sup>4</sup>Centre for the Analysis of Genome Evolution and Function, University of Toronto, Toronto,  
14 Ontario, Canada

15 <sup>5</sup>Division of Infectious Diseases, Department of Medicine, University Health Network, University  
16 of Toronto, Toronto, Ontario, Canada

17 <sup>6</sup>Adult Cystic Fibrosis Clinic, St. Michael's Hospital, Toronto, Ontario, Canada

18 <sup>7</sup>Department of Pediatric Laboratory Medicine, Division of Microbiology, The Hospital for Sick  
19 Children, Toronto, Ontario, Canada

20 <sup>8</sup>Department of Pediatrics, Division of Infectious Diseases, The Hospital for Sick Children,  
21 University of Toronto, Toronto, Ontario, Canada

22 <sup>9</sup>Department of Pathology, University Health Network, Toronto, Ontario, Canada.

23  
24 \*To whom correspondence may be addressed. Email: [david.guttman@utoronto.ca](mailto:david.guttman@utoronto.ca)

25  
26  
27 Running title: *B. multivorans* GWAS reveals a role for recombination in the evolution of  
28 antimicrobial resistance

29  
30  
31 Keywords: *Burkholderia multivorans*, cystic fibrosis, evolution, genome wide association  
32 analyses, bacterial population dynamics, recombination

33 **Abstract** (300 words)

34

35 Cystic fibrosis (CF) lung infections caused by members of the *Burkholderia cepacia* complex,  
36 such as *Burkholderia multivorans*, are associated with high rates of mortality and morbidity. We  
37 performed a population genomic study of 111 *B. multivorans* sputum isolates from a single CF  
38 patient through three stages of infection including the initial incident infection, deep sampling of  
39 a one-year period of chronic infection, and deep sampling of a post-transplant recolonization.  
40 We reconstructed the evolutionary history of the population and used a lineage-controlled  
41 genome-wide association study (GWAS) approach to identify genetic variants associated with  
42 antibiotic resistance. We found that the incident isolate was more susceptible to agents from  
43 three antimicrobial classes ( $\beta$ -lactams, aminoglycosides, quinolones), while the chronic isolates  
44 diversified into distinct genetic lineages with reduced antimicrobial susceptibility to the same  
45 agents. The post-transplant reinfection isolates displayed genetic and phenotypic signatures  
46 that were distinct from sputum isolates from all CF lung specimens. There were numerous  
47 examples of parallel pathoadaptation, in which individual loci, or even the same codon, were  
48 independently mutated multiple times. This set of loci was enriched for functions associated with  
49 virulence and resistance. Our GWAS approach identified one variant in the *ampD* locus (which  
50 was independently mutated four times in our dataset) associated with resistance to  $\beta$ -lactams,  
51 and two non-synonymous polymorphisms associated with resistance to both aminoglycosides  
52 and quinolones, affecting an *araC* family transcriptional regulator, which was independently  
53 mutated three times, and an outer member porin, which was independently mutated twice. We  
54 also performed recombination analysis and identified a minimum of 14 recombination events.  
55 Parallel pathoadaptive loci and polymorphisms associated with  $\beta$ -lactam resistance were over-  
56 represented in these recombinogenic regions. This study illustrates the power of deep,  
57 longitudinal sampling coupled with evolutionary and lineage-corrected GWAS analyses to reveal  
58 how pathogens adapt to their hosts.

59 **Author Summary**

60

61 Cystic fibrosis (CF) is a common lethal genetic disorder that affects individuals of European  
62 descent and predisposes them to chronic lung infections. Among the organisms involved in  
63 these infections, bacteria from the *Burkholderia cepacia* complex (BCC) are often associated  
64 with poor clinical prognosis. This study examines how the most prevalent BCC species among  
65 CF patients, *B. multivorans*, evolves within a CF patient and identifies mutations underlying  
66 antibiotic resistance and adaptation to both the native CF lung and a non-CF lung allograft. We  
67 demonstrate that *B. multivorans* can diversify phenotypically and genetically within the CF lung,  
68 with a complex population structure underlying a chronic infection. We noted that isolates  
69 collected after the patient was re-infected post-transplant were more closely related to  
70 descendants of the incident clone than to those recovered in the weeks prior to transplant. We  
71 used a genome-wide association method to identify genes associated with resistance to the  $\beta$ -  
72 lactam antibiotics: aztreonam and ceftazidime. Many of these variants were found in regions  
73 that show patterns of recombination (genetic exchange) between strains. We also found that  
74 genes which were mutated multiple times during overall infection were more likely to be found in regions  
75 showing signals consistent with recombination. The presence of multiple independent  
76 mutations in a gene is a very strong signal that the gene helps bacteria adapt to their  
77 environment. Overall, this study provides insight into how pathogens adapt to the host during  
78 long-term infections, specific genes associated with antibiotic resistance, and the origin of new  
79 and recurrent infections.

80 **Introduction**

81  
82 The *Burkholderia cepacia* complex (BCC) describes a highly diverse group of at least 20 closely  
83 related species within the genus *Burkholderia* that can cause serious opportunistic infections in  
84 humans [1, 2]. Individuals with the fatal genetic disease cystic fibrosis (CF) are particularly  
85 susceptible to chronic BCC infections, which are commonly associated with rapid decline in lung  
86 function, high rates of mortality and poor post-transplant outcome [3, 4]. Of the BCC species,  
87 *Burkholderia multivorans* and *Burkholderia cenocepacia* account for 85-97% of all BCC found in  
88 CF patients [5]; however, *B. multivorans* infections have surpassed *B. cenocepacia* in  
89 prevalence over the past decade [6]. Many BCC that are CF-associated are intrinsically virulent  
90 and antibiotic resistant and require strict infection control practices, as they can be transmitted  
91 between patients [7-10]. Despite a wealth of knowledge describing the molecular basis of these  
92 pathogenic properties and their evolution in strains of the well-studied *B. cenocepacia*, little is  
93 known about the factors that govern these attributes in *B. multivorans* [9].

94  
95 Dissecting the molecular basis of complex adaptive traits in bacterial pathogens, such as  
96 antimicrobial resistance, can be difficult as a single phenotype may be influenced by a large  
97 number of loci that interact with each other as well as their environment. Resistance in the BCC  
98 is associated with alterations to outer membrane permeability, the expression of multidrug efflux  
99 pumps and  $\beta$ -lactamases, and diversification of antimicrobial targets [11]. Consequently,  
100 methods that focus on identifying polymorphisms in single genes with large effects may miss the  
101 majority of loci that modulate phenotypes in more subtle ways. The development of genome-  
102 wide association studies (GWAS) has expanded our ability to identify loci of small effect size  
103 that have been associated with numerous diseases and other related phenotypes of interest in  
104 humans [12, 13]. In contrast, the application of GWAS to analyze bacterial behaviors has been  
105 slower to gain traction for a number of inter-related reasons: 1) clonal reproduction of microbes  
106 leads to confounding associations due to common ancestry, often referred to as population  
107 structure; 2) recombination in bacteria, which is more analogous to gene conversion than  
108 eukaryotic recombination, occurs at variable rates among different species and is not linked to  
109 reproduction; 3) the unpredictable nature of recombination results in the erratic breakdown of  
110 linkage disequilibrium between selected sites and distal neutral sites; and 4) selection can be  
111 extremely strong, resulting in the relatively rapid fixation of not only a selected allele, but entire  
112 genomes due to the linkage disequilibrium [14, 15].

113

114 Nevertheless, several recent studies have proposed novel approaches to overcome these  
115 challenges. These methods include using cluster membership [16-18], phylogenetic history [15,  
116 19, 20], or lineage effects [21] to differentiate mutations leading to a phenotypic outcome from  
117 mutations related to the genetic background of the bacterial population. While these methods  
118 hold tremendous promise for identifying genetic variation underlying bacterial phenotypes of  
119 interest, they generally focus on cross sectional sampling of diverse isolates and populations.  
120 Their power has not been established for the fine-scale analysis of individual bacterial  
121 populations evolving over short time scales, with strong positive selection and restricted  
122 recombination [14, 22]. The application of fine-scale evolutionary analysis to bacterial  
123 populations is especially important in the context of clinically significant pathogen infections,  
124 where evolution is associated with adaptation to the host environment and antimicrobial  
125 treatment [23].

126

127 In this study, we take a fine-scale approach to microbial GWAS to examine the genetic basis of  
128 antimicrobial resistance within a *B. multivorans* population that had been sampled longitudinally  
129 from a single patient over a ten-year period. We characterized the genomic diversity in this  
130 population and assessed associations between all genetic variants and multiple antibiotic  
131 resistance phenotypes. Using a clustering-based approach to control for population structure  
132 and linkage disequilibrium, our analysis identified single nucleotide polymorphisms (SNPs) that  
133 were associated with resistance to  $\beta$ -lactams, aminoglycosides, and quinolones. In addition, we  
134 found that both multiply-mutated loci (those that are targets of parallel pathoadaptation) and  $\beta$ -  
135 lactam resistance-associated variants were overrepresented in recombinogenic regions of the  
136 *B. multivorans* genome

137

## 138 **Results**

139

140 For our evolutionary analysis and GWAS, we used a series of *B. multivorans* isolates that were  
141 cultured from respiratory specimens obtained from an adult male with CF (CF170, being  
142 followed by the CF Clinic at St. Michael's Hospital, Toronto, Canada). In a ten-year period,  
143 patient CF170 acquired an incident (i.e. initial) lung *B. multivorans* infection, developed a  
144 chronic *B. multivorans* lung infection, received a double lung transplant, and finally experienced  
145 a *B. multivorans* re-colonization of the allograft three years post-transplant. Isolates from each  
146 of these three phases of his *B. multivorans* infection are represented in this study (Fig 1). We  
147 defined these isolates as 1) the single isolate recovered from the patient's first infection – the

148 'incident infection' isolate; 2) 100 isolates collected six to seven years post-incident infection  
149 from ten sputum specimens (ten isolates per specimen) over approximately a one-year period –  
150 the 'chronic infection' isolates; and 3) ten isolates collected from a single expectorated sputum  
151 sample ten years after the incident infection, and three years after the patient underwent a  
152 double lung transplant – the 'post-transplant' isolates. Patient CF170 was being treated with  
153 alternating cycles of antibiotic therapy while chronically infected, with 13 antibiotics being  
154 administered at different intervals and durations over the course of the chronic infection  
155 sampling period (Fig 1). The genomes of all 111 isolates were whole-genome sequenced on the  
156 Illumina platform, yielding a median coverage depth of 117X (S1 Fig). Multi-locus sequence  
157 typing was performed *in silico* by extracting seven loci from the whole genome sequence data  
158 (*atpD*, *gltB*, *gyrB*, *recA*, *lepA*, *phaC*, *trpB*) and comparing them to the *Burkholderia cepacia*  
159 complex MLST Databases in pubMLST. This analysis revealed that all isolates were clonally  
160 related and of the sequence type ST-783 [24].  
161

162 **Genomic diversity and phylogenetic analysis suggest underlying population structure.**  
163 The *de novo* genome assembly of a single isolate recovered from the third chronic infection  
164 sputum sample was used as the reference for the mapping assembly of all other isolates. This  
165 particular isolate was chosen as the reference since it had the best overall *de novo* assembly  
166 metrics. The reference assembly consisted of 6,444,123 bases across 26 contigs, which were  
167 pseudo-scaffolded against the complete genome of *B. multivorans* ATCC 17616 (Fig 2A).  
168 Through a conservative variant calling pipeline [25], a total of 1,892 SNPs and 328 indels  
169 segregating among the 111 isolates were identified, with 1,039, 672, and 180 SNPs being found  
170 on chromosomes, 1, 2, and 3 respectively. Only a single SNP was found in a contig which did  
171 not map to the ATCC 17616 genome. Overall, 740 (39.1%) SNPs and 163 (49.9%) indels were  
172 parsimonious informative (PI, i.e. non-singleton), and 226 (11.9%) SNPs and 99 (30.2%) indels  
173 segregated in at least two sampling time points. From the 1,892 SNPs, 70.5%, 15.6%, and  
174 13.9% were non-synonymous, synonymous, and intragenic substitutions respectively (Fig 2C).  
175 52.1% of the intergenic SNPs were found in putative regulatory regions (defined as the  
176 intergenic region within 150 bases from the start codon of any gene). The population showed a  
177 genetic diversity average of  $123.62 \pm 120.98$  (number of SNP differences, mean  $\pm$  standard  
178 deviation) pairwise differences. The distribution of these difference suggested an underlying  
179 population structure since genetic diversity was not uniform even among isolates from the same  
180 specimen (S2 Fig).  
181

182 We reconstructed the core genome phylogenetic relationships among all isolates using an  
183 alignment of the 1,892 SNPs and a Bayesian approach (Fig 3A). The root of this tree was  
184 identified by adding *B. multivorans* ATCC17616 to the analysis. The tree topology indicates that  
185 the incident infection isolate diverged from the other 110 isolates at the base of the tree. The ten  
186 isolates from the post-transplant sample are again highly divergent (relative to the total diversity)  
187 and form a basally branching, monophyletic clade, while the chronic sample isolates form a less  
188 divergent, monophyletic clade. Moreover, there seem to be subgroups among the chronic  
189 infection isolates suggesting population structure. This structure is also observed in a network-  
190 based phylogenetic approach (S3 Fig), where two groups of isolates from the chronic infection  
191 sampling cluster in a star-like phylogeny. Star phylogenies are characterized by roughly equal  
192 divergence from the common ancestor, and are associated with recent purges in genetic  
193 variation [26].

194

195 **Population structure analysis clusters the isolates into five groups.** We used the Monte  
196 Carlo Markov Chain analysis of SNPs and indels implemented in STRUCTURE to infer  
197 population structure among the 111 isolates. We identified the lowest number of subpopulations  
198 that maximized the likelihood of data; hence determining the underlying population structure in  
199 the data without overestimating the number of subpopulations [27]. There were three  
200 subpopulations that arose from single common ancestors, which we labelled groups R, B, and  
201 G, comprising 54, 26, and 10 isolates, respectively (Fig 3C-D). The ancestral composition of  
202 the incident isolate and seven of the chronic infection isolates, recovered at collection points T1,  
203 T2 and T10, resembled a combination of the three identified subpopulations. This group of  
204 isolates was labeled RBG. Another group labeled RB (13 isolates) has an admixed ancestry  
205 from the ancestral subpopulations of R and B.

206

207 Isolates from groups RBG and RB were found in low frequencies through different samples from  
208 the chronic infection period (Fig 3B). In contrast, isolates from group R or B were more  
209 dominant in this same period. The isolates from group R were first observed at the third time  
210 point of the chronic infection samples, and they remained the most abundant group in  
211 subsequent chronic samples (Fig 4). In contrast, the abundance of group B isolates decreased  
212 over time. The genetic diversity, measured as number of SNPs, significantly differed between  
213 these groups (one-way ANOVA:  $F(4,1902) = 1,426.133$ , p-value < 0.0001), with group G (those  
214 recovered exclusively post-transplant) being the most diverse, followed by groups RBG and RB,  
215 then groups R and B (S4a Fig).

216

217 The time to the most recent common ancestor (tMRCA) calculated as days before the last  
218 sample for all isolates and the various STRUCTURE-defined groups is shown in Supplementary  
219 Figure 4c. This analysis shows that the RGB group, which includes all of the chronic infection  
220 isolates as well as the post-transplant isolates, coalesced to a common ancestor at roughly the  
221 same time as the full isolate collection, including the incident infection (S4c Fig). This result  
222 supports the hypothesis that the infection of the transplanted lung came from the same source  
223 as the original incident isolate, despite being separated by approximately ten years, as opposed  
224 to a clone that persisted and diversified in the lung of the patient during chronic colonization.  
225 Additionally, it appears that groups R and B diverged at approximately the same time (S4c Fig).  
226 Unfortunately, we are unable to determine if these were allopatric populations that colonized  
227 distinct regions in the lung, or sympatric populations that coexisted within the same  
228 compartment due to our sampling of expectorated sputum.

229

230 **Selection analysis supports positive selection in the population.** We determined the ratio  
231 of non-synonymous to synonymous substitutions ( $d_N/d_S$ ) as an estimate of selection. Since we  
232 expect that time has allowed natural selection or genetic drift to have acted on the multi-time  
233 segregating mutations more so than on variants that segregate in a single sample, we  
234 determined the  $d_N/d_S$  both for all SNPs in each group, as well as for only those that segregate in  
235 at least two time-points – ‘multi-time’ SNPs (S4b Fig). The  $d_N/d_S$  for the overall population was  
236 1.35 (95% confidence interval, CI = 1.19-1.53) and 1.34 for multi-time SNPs (CI = 0.94-1.96),  
237 which may indicate weak positive selection, or simply the segregation of mildly deleterious  
238 variants. Only groups R and RB multi-time SNPs showed  $d_N/d_S$  above the neutral expectation  
239 of 1.0 (group R  $d_N/d_S$  = 2.05, CI = 0.57-11.15, group RB  $d_N/d_S$  = 2.38, CI = 1.08-6.18), although  
240 the confidence intervals for the group R are quite large. All other groups had  $d_N/d_S$  ratios only  
241 slightly elevated (ranging from 1.04-1.63), although the differences between groups were not  
242 statistically significant.

243

244 Further support for positive selection comes from a significantly negative Tajima's D test ( $D = -$   
245  $2.21$ ,  $P < 0.01$ ) and Fu and Li's tests ( $D^* = -6.11$ ,  $P < 0.02$ ;  $F^* = -5.20$ ,  $P < 0.02$ ). While all three  
246 of these results can be explained by both positive selection and recent population expansion,  
247 the combination of these results with the high nucleotide diversity and  $d_N/d_S > 1.0$  is most  
248 consistent with positive selection.

249

250 **GWAS identification of variants associated with antibiotic resistance.** We assumed that  
251 the intensive antibiotic exposure during the chronic infection sampling period would result in  
252 strong selection for resistance-associated genotypes in *B. multivorans*. Minimum inhibitory  
253 concentrations (MICs) for two  $\beta$ -lactams (aztreonam, ceftazidime), two aminoglycosides  
254 (tobramycin and amikacin), and the fluoroquinolone ciprofloxacin were determined for all  
255 isolates. Isolates from the three phases of infection had distinct susceptibility profiles. The  
256 incident isolate had MICs of 8  $\mu$ g/mL or less for all agents tested, while all chronic infection and  
257 post-transplant isolates had higher MICs for both aminoglycosides (t-test  $p < 0.0001$ , Fig 3E),  
258 but variable MICs for  $\beta$ -lactams and fluoroquinolone tested (range:  $\leq 8$  to  $>512$   $\mu$ g/mL).

259  
260 The 1,892 SNP positions segregating among the 111 isolates were grouped in 150 distinct  
261 mutational profiles (i.e. one or more SNP positions that share the same pattern of reference vs.  
262 alternative base among the strain collection, S5 Fig). Prior to population control, each of these  
263 mutational profiles was examined for a statistical association to the five tested antibiotics at six  
264 different levels of resistance and these associations were corrected for multiple testing by taking  
265 into consideration the number of tests. Five mutational profiles (comprising 17 SNPs)  
266 associated with resistance to both  $\beta$ -lactam antibiotics, and one mutational profile (comprising 2  
267 SNPs) associated specifically with ceftazidime (S6 and S7 Fig). Ten mutational profiles  
268 (comprising 250 SNPs) were associated with resistance to amikacin, tobramycin, and  
269 ciprofloxacin. Additionally, two mutational profiles (comprising 31 SNPs) associated with  
270 resistance to both aminoglycosides, and four mutational profiles (comprising 33 SNPs)  
271 associated specifically with ceftazidime.

272  
273 Next, we tested these variants against population structure controls, counting only those  
274 associated variants that were observed in multiple subpopulation groups as determined by the  
275 population structure analysis. This criterion could be satisfied by one of two mechanisms: 1) the  
276 mutations arose in the subpopulations through multiple independent mutational events, or 2)  
277 they arose in a common ancestor of multiple subpopulations and have been maintained in  
278 multiple lineages while being lost in others. Out of all mutational profiles associated with  
279 elevated MICs for both  $\beta$ -lactams, one (comprising a single SNP) passed the population  
280 structure control (S6b Fig). This SNP was found in 20.4% of isolates in group R, and 50% of  
281 isolates in group RBG. This variant leads to a non-synonymous amino acid substitution in the  
282 sequence of the *ampD* gene (BMUL\_2790), a locus extensively studied for its role in resistance  
283 to  $\beta$ -lactams [28, 29]. This mutation was predicted to have a deleterious effect on AmpD by

284 PROVEAN analysis (score = -8.0, S8a Fig). In fact, the *ampD* locus was independently mutated  
285 four other times within our dataset. A second SNP in *ampD* was found in a mutational profile  
286 that was similarly associated with  $\beta$ -lactam MICs; nevertheless, it failed to pass the population  
287 structure control. Additionally, two mutational profiles associated to the aminoglycosides and  
288 ceftazidime showed evidence of multiple independent polymorphic events (S6e Fig). One of  
289 these mutational profiles, which comprises a single SNP, is represented by a non-synonymous  
290 substitution in an *araC* family transcriptional regulator locus (BMUL\_3951). PROVEAN analysis  
291 indicates that this mutation is unlikely to have a deleterious effect on the locus (score = 6.906).  
292 The second mutational profile, again including only a single SNP, gave rise to a non-  
293 synonymous substitution in locus BMUL\_3342, which is annotated as an outer member protein  
294 (porin). While this mutation is not expected to end in a deleterious effect (PROVEAN score =  
295 3.273), it occurs in a locus that is independently mutated two other times.

296

297 **Additional variants associated with pathoadaptation can be detected by identifying multi-**  
298 **mutated loci.** Loci that are independently mutated multiple times provide strong evidence of  
299 selection by parallel pathoadaptation [30]. We observed 328 loci that were independently  
300 mutated multiple times in our collection (Table 1). Given the genome size and the total number  
301 of polymorphisms (both SNPs and indels), we only consider the 62 loci with three or more  
302 independent mutations to be statistically significant ( $p$ -value  $< 0.05/[1,892 \text{ SNPs} + 328 \text{ indels} =$   
303 2220 polymorphisms]). 184 SNPs (9.7%) and 26 indels (7.9 %) were found in these 62 loci. We  
304 excluded the possibility that multiply mutated loci showed excess polymorphism simply due to  
305 an increased mutational rate by examining the mutational class spectrum for the multiply  
306 mutated loci relative to the genome-wide average. While the rate of non-synonymous,  
307 synonymous and intergenic mutations among all 1,892 SNPs is 70.5%, 15.6%, and 13.9%  
308 respectively, the mutational class spectrum of the SNPs found among multiply mutated loci is  
309 83.1% non-synonymous, 11.7% synonymous, and 3.2% intergenic substitutions. Therefore, the  
310 mutational class distribution of SNPs found in multiply mutated loci is significantly skewed  
311 toward an excess of non-synonymous mutations ( $P < 0.0001$ , chi-square test).

312

313 Some of these multi-mutated loci are known to play significant roles in antibiotic resistance. For  
314 example, a gene encoding a probable transcriptional regulator protein of MDR efflux pump  
315 cluster (BMUL\_0641), which has been associated with drug resistance in multiple pathogens  
316 [31-33], has seven independently acquired mutations, and the probability of any gene being  
317 mutated seven times is  $1.65 \times 10^{-23}$ . A locus with five multiple mutations ( $P = 6.48 \times 10^{-16}$ ) encodes

318 N-acetylmuramoyl-L-alanine amidase (AmpD, BMUL\_2790), which is associated with resistance  
319 to  $\beta$ -lactam antibiotics [28]. Moreover, a functional enrichment analysis revealed the  
320 phosphorelay signal transduction system GO function overrepresented in multiply mutated  
321 genes compared to the functional annotation of the whole genome ( $P = 0.050$ ). The  
322 phosphorelay signal transduction system has been previously described as a therapeutic target,  
323 given that it controls the expression of genes encoding virulence factors [34].

324

325 We also found ten genes that had two independent mutations located in the same or adjacent  
326 codon (Table 2). The mutational class spectrum of the SNPs associated with this observation is  
327 of 90%, 10% and 0% of non-synonymous, synonymous, and intergenic substitutions,  
328 respectively. In this case, the fraction of non-synonymous mutations is significantly higher than  
329 the fraction found for both all SNPs, as well as all the SNPs in the multiply mutated loci ( $P <$   
330 0.00001, chi-square test). One of the genes with multiple independent mutations in the same  
331 codon encodes for RNA polymerase sigma factor (RpoD), which is associated with the  
332 expression of housekeeping genes [35]. One of the mutations in this locus is fixed between the  
333 post-transplant isolates and the rest of the isolates, and the other mutation is fixed between the  
334 isolates in group RBG collected in the tenth sample time and the rest of the isolates.

335

336 **Parallel pathoadaptive variants are overrepresented in recombinogenic regions.** We  
337 identified a minimum of 14 recombination events in our full dataset based on the four-gamete  
338 tests of Hudson and Kaplan [36] (Fig 2D). Three of these events were identified between sites in  
339 different genome assembly contigs; therefore, they were not considered in downstream  
340 recombination analysis. The nucleotide length of these recombinogenic regions ranged from  
341 4,783 bases to 192,532 bases, and these regions account for 15.1% of the assembled genome.  
342 300 (15.9%) out of the total 1,892 SNPs and 47 indels (14.3%) occur in these regions, which is  
343 not significantly different than expected given the recombinogenic proportion of the genome.

344

345 We next looked to see if there was an association between recombination and the evolution of  
346 antibiotic resistance. 51 (18.3%) of the 279 SNPs associated with both aminoglycosides tested  
347 (amikacin & tobramycin), and 42 (14.9%) of the 281 SNPs linked to ciprofloxacin are found in  
348 recombinogenic regions (Fig 5A). These ratios fail to reject the null hypothesis that these  
349 mutations are randomly distributed around the genome. On the other hand, 52.9% (9 of 17  
350 SNPs) and 47.4% (9 of 19 SNPs) of the SNPs associated with aztreonam and ceftazidime,

351 respectively, are found in recombinogenic regions, which are significantly different than  
352 expected by chance ( $p < 0.0001$ , chi square test).

353

354 Finally, 49 (26.6%) of the 184 SNPs and 4 (8.5%) of the 47 indels found in loci independently  
355 mutated three or more times occur in the identified recombinogenic regions (Fig 5B). Thus,  
356 while SNPs involved in multi-mutated loci are overrepresented in recombinogenic regions more  
357 than expected ( $P < 0.0001$ , chi square test), indels in multi-mutated genes are not significantly  
358 underrepresented.

359

## 360 Discussion

361

362 Our study investigated how *B. multivorans* evolves within the lungs of an individual afflicted with  
363 CF using a deep longitudinal sampling design (i.e. multiple isolates obtained per sputum  
364 sample) to capture both the overall population diversity and the temporal shifts that occurred at  
365 different phases of the infection, including the colonization of a new allograft. To identify the  
366 source of genetic diversity in this *B. multivorans* population, we needed to understand: 1) the  
367 genetic relationships between the incident isolate that was recovered from the first BCC-positive  
368 sputum culture, the chronic strains that persisted in the population, and the population of strains  
369 that re-established an infection post-transplant; 2) whether there were multiple colonization  
370 events of the patient by divergent clones; 3) how genetic diversity was generated and dispersed  
371 in the population; and 4) how the pathogen adapts and responds to clinical treatment. While we  
372 were unable to address all of these questions, we have concluded that the chronic population  
373 originated from either the incident isolate, or a clone that shared a recent common ancestor with  
374 the incident isolate. Furthermore, all of the chronic isolates descended from a single common  
375 ancestor, ruling out multiple independent colonization events.

376

377 One clear signal is that the *B. multivorans* isolates recovered from the post-transplant lung did  
378 not originate from the chronic population. In fact, it appears that the post-transplant isolates  
379 came from a new infection that originated from the same source as the incident infection.  
380 Unfortunately, the source of these infections cannot be determined, and could be either the  
381 environment or the patient's upper respiratory tract. In the former case, it is likely that the patient  
382 lived in the same home or locale over the course of the study, and that the ancestral *B.*  
383 *multivorans* clone is endemic in that environment. Alternatively, in the latter case, the upper  
384 respiratory tract is known to act as a reservoir for a number of CF pathogens [37].

385 Consequently, it is possible that clonal descendants of the ancestral or incident strains resided  
386 in the patient's upper airways since the incident infection. Some transplant procedures attempt  
387 to clean the nasal reservoir prior to transplant via nasal washing / scraping, but we do not know  
388 if this was done for this patient. If this hypothesis is true, it would explain why the post-transplant  
389 isolates have an antibiotic susceptibility pattern much more similar to the chronic isolates than  
390 the incident isolate. We also note that the post-transplant population is much more genetically  
391 diverse than any of the chronic populations. This could suggest that this population was rapidly  
392 adapting to an environmental change, such as the shift from CF to non-CF conditions, which  
393 would include, differences in immune response, the composition of the allograft microbiome,  
394 and treatment regimens. Alternatively, it could reflect colonization by a population of related  
395 strains. It is possible that given sufficient time this population would eventually be winnowed  
396 down to a single surviving clone (as is seen with the incident infection) due to selection and / or  
397 genetic drift

398

399 A major motivator for this study was to better understand how pathogens adapt to their hosts  
400 over the course of disease progression and treatment; an issue that can be addressed using  
401 statistical association tests. Correcting for the genetic structure of the bacterial population poses  
402 a challenge to the implementation of these tests. Population structure in this context refers  
403 relationships among strains due to descent from a common ancestor and limited recombination.  
404 This structure results in the linkage of segregating genetic variation around the genome, which  
405 makes it very difficult to distinguish a causal mutation that is responsible for a phenotype of  
406 interest from a neutral variant that occurred in the same genetic background. In the absence of  
407 recombination, the neutral mutation will have the same population distribution as the causal  
408 mutation due to genetic hitchhiking. This issue is particularly prevalent when studying largely  
409 isolated and recently evolved populations, such as the case of pathogens evolving within a host.  
410

411 To overcome these two issues, we imposed a lineage control filter on our GWAS approach, in  
412 which we focused only on mutations that occurred in multiple, distinct, genetic lineages. This  
413 pattern can best be explained by recombination of polymorphisms between lineages, but  
414 formally, could also be due to extensive gene loss. Our analysis showed that linkage  
415 disequilibrium was only disrupted in a relatively small number of polymorphism (those  
416 polymorphisms shown as orange circles; S7b-e Fig). This reinforces the need for deep sampling  
417 since the infrequent recombination signals may have been missed if isolates were only collected  
418 from a single sample, or if only single isolates were recovered from each sample. Consequently,

419 the tractability of GWAS in this *B. multivorans* population was greatly enhanced by our sampling  
420 schema.

421

422 Using the established lineage structure of the *B. multivorans* population as control for our  
423 association study, we identified two non-synonymous SNPs associated with resistance to the  
424 aminoglycosides amikacin and tobramycin, and to the quinolone ciprofloxacin. One of these  
425 SNPs occurs in a locus encoding the transcription factor AraC, which is involved in the global  
426 regulation of efflux pumps, while the other SNP was found in a locus annotated as a porin.  
427 Although not specific to aminoglycosides or quinolones, overexpression of efflux pumps and  
428 repression of porin proteins has been reported as important mechanisms of antibiotic resistance  
429 for bacteria [38]. Neither mutation is projected to significantly vary the function of the encoding  
430 protein.

431

432 Additionally, we identified a single SNP associated with resistance to the  $\beta$ -lactams aztreonam  
433 and ceftazidime. This SNP occurs in the *ampD* gene, which is a negative regulator of the  $\beta$ -  
434 lactamase AmpC, and it is expected to have a deleterious effect in the encoding protein. This  
435 observation is not unexpected as bacteria treated with  $\beta$ -lactams would benefit from the  
436 constitutive overproduction of  $\beta$ -lactamase. Overall, AmpD seems to play an important role in  
437 the pathoadaptation of this *B. multivorans* population since four other independent non-  
438 synonymous mutations, all of which are expected to have deleterious effects on the protein,  
439 occur at this locus (S8a Fig).

440

441 Our use of the population control criterion of only considering mutations present in multiple  
442 lineages meant that we excluded some variants associated to virulence, such as one of the four  
443 mutations in *ampD*, which was statistically associated with  $\beta$ -lactam resistance. Without our  
444 population control it would be impossible to identify causative mutations from hitchhiking  
445 variants that are in linkage disequilibrium with the causative mutation. Filtering in this manner  
446 reduces the number of false positives; nevertheless, variants underlying phenotypes of interest  
447 could be segregating in linkage disequilibrium blocks, and therefore, may not be identified in our  
448 GWAS approach (false negatives).

449

450 We observed that mutations associated with resistance to  $\beta$ -lactams (prior to lineage controls)  
451 occur disproportionately in recombinogenic regions (Fig 2F), while variants associated with both  
452 aminoglycosides or ciprofloxacin are more randomly distributed with respect to recombinogenic

453 regions. The study patient received both long-term maintenance  $\beta$ -lactam and aminoglycoside  
454 treatments in addition to multiple short-term  $\beta$ -lactam treatments that included cycles of  
455 ceftazidime, piperacillin/tazobactam, meropenem, and cefepime. This more aggressive and  
456 varied course of treatment with  $\beta$ -lactams could potentially explain the increased role of  
457 recombination in the dissemination of putatively beneficial polymorphisms, similar to what has  
458 been observed in other pathogens [39, 40].

459

460 Our analysis identified genes under strong selection by focusing on loci with a statistical excess  
461 of independent mutations (i.e. parallel pathoadaptation) [25, 41, 42]. Examining multi-mutated  
462 loci can reveal the heterogeneous selective pressures that bacteria must adapt to in order to  
463 reside within the lung. For instance, a gene encoding a transcription regulator of multidrug  
464 resistance efflux pumps independently accumulated seven different mutations leading to eight  
465 unique alleles in our population of 111 *B. multivorans* isolates. We also found seven different  
466 alleles of a locus encoding cyclic  $\beta$ -1,2-glucan synthase, which is linked to bacteria's ability to  
467 elude host cell defenses [43]. A number of loci underlying virulence-associated traits, such as  
468 quorum sensing and biofilm production, also carry multiple independent mutations. Particularly  
469 interesting are multiply mutated loci with no characterized function, or with no prior linkage to  
470 resistance or virulence. These loci include a NAD-glutamate dehydrogenase locus BMUL\_4010,  
471 which was mutated five independent times over the course of the study, and a glycosyl  
472 transferase protein (BCEN2424\_5592), not previously seen in *B. multivorans* that was mutated  
473 six times (4 SNPs and 2 indels) during the course of the study. Examples such as these provide  
474 excellent candidates for characterizing the cryptic resistome – loci previously not known to be  
475 involved in antimicrobial resistance. In addition, the strongest signals of parallel pathoadaptation  
476 involve those cases where mutations occur independently in the same or adjacent codon.  
477 These observations point to a very specific form of selective pathoadaptation, which identifies  
478 the specific residue or region of the locus that potentially plays a role in selective advantage and  
479 may affect a conserved function.

480

481 Finally, our study highlighted an intriguing role for recombination in the development of  
482 antimicrobial resistance in *B. multivorans*. We observed that multi-mutated loci were over-  
483 represented within recombinogenic regions, along with an excess of mutations associated with  
484  $\beta$ -lactam resistance. This suggests that while recombination plays an important role in the  
485 pathoadaptation of this *B. multivorans* population, its selective benefit may be environment  
486 dependent.

487

488 Our study illustrates the relevance of deep, longitudinal sampling to the implementation of  
489 GWAS approaches in a population under positive selection. We identified the potential genetic  
490 basis behind the antibiotic resistance of a *B. multivorans* population in a single host. Moreover,  
491 this approach allowed us to study variants associated to antibiotic resistance and revealed that  
492 resistance to  $\beta$ -lactams may be passed within the population via recombination. This study is  
493 limited to *in silico* predictions of the impact mutations on protein function, and future efforts  
494 should include functional validation of these mutants; nevertheless, many of the identified genes  
495 are already well-established targets for antibiotic resistance. Additionally, our findings are  
496 restricted to a single patient and a single bacterial species; extending this approach in other  
497 systems under positive selection will be required to establish the generalizability of the findings.  
498 Nevertheless, this study is one of the first examining in depth the fine-scale evolution of *B.*  
499 *multivorans* in the lungs of a CF patient as it transitions from an early infection to chronic  
500 infections and the eventual reinfection of a transplanted allograft.

501

502 **Materials and Methods**

503

504 **Ethics statement.** All protocols involving the collection, handling and laboratory use of  
505 respiratory specimens were approved by the Research Ethics Boards of St. Michael's Hospital  
506 (Protocol #09-289) (Toronto, Canada) and the University Health Network (Protocol #09-0420-T)  
507 (Toronto, Canada). We obtained informed consent from the study subject prior to specimen  
508 collection and sputa were produced voluntarily. All experiments involving clinical specimens  
509 were performed in accordance with the *Tri-Council Policy Statement: Ethical Conduct for*  
510 *Research Involving Humans*, of the Canadian Institutes of Health Research, the Natural  
511 Sciences and Engineering Research Council of Canada, and the Social Sciences and  
512 Humanities Research Council of Canada.

513

514 **Specimen collection and isolation of *B. multivorans*.** Sputum specimens were collected by  
515 expectoration from a 29-year-old male (CF170), with a homozygous  $\Delta F508$  CFTR genotype  
516 being followed at the Adult CF Clinic at St. Michael's Hospital (Toronto, Canada). Ten sputum  
517 specimens were collected over a 10-month period while the patient was in the advanced stages  
518 of CF lung disease (assessed by the forced expiratory volume in 1 second (FEV<sub>1</sub>), FEV<sub>1</sub> which  
519 was 27-39 % predicted throughout the course of the study), and an additional sputum specimen  
520 obtained after the patient had undergone double lung transplantation. All specimens were  
521 processed for bacterial culture as previously described [44]. After 48h of incubation, cultures  
522 were visually inspected, and each distinct colony morphotype was described using eight  
523 characteristics of physical appearance (pigmentation, size, surface texture, surface sheen,  
524 opacity, mucoidy, autolysis and margin shape). Ten colonies were selected from each sputum  
525 culture in relation to the diversity of colony types present. The incident isolate was obtained from  
526 the *Burkholderia cepacia* complex repository at St. Michael's Hospital and was recovered from  
527 the first BCC positive sputum culture produced by the study patient (Toronto, Canada). Isolates  
528 were stored at -80°C in 20% (v/v) glycerol after a 20h subculture in LB broth (Wisent Inc., QC,  
529 CA) and confirmed as *Burkholderia* spp. by a secondary subculture onto both *Burkholderia*  
530 *cepacia* selective (BCSA) (HiMedia Laboratories, Mumbai, IN) and MacConkey (Becton  
531 Dickinson, MD, USA) agars, as well as being tested for growth at 42°C. The *recA* gene was  
532 sequenced from each isolate as described by Spilker *et al.* for preliminary speciation [45].

533

534 **Antimicrobial susceptibility testing.** Each isolate confirmed as *B. multivorans* was screened  
535 for antimicrobial susceptibility by agar dilution using Clinical and Laboratory Standards Institute

536 procedures [46]. We tested susceptibility to representatives of the  $\beta$ -lactam (aztreonam [ATM],  
537 ceftazidime [CAZ]), fluoroquinolone (ciprofloxacin [CIP]) and aminoglycoside (amikacin [AMK],  
538 tobramycin [TOB]) (Sigma-Aldrich, ON, Canada) classes. Minimum inhibitory concentrations  
539 (MIC), defined as the lowest concentration of each antibiotic to inhibit growth, were reported as  
540 the median MIC of three independent experiments. Growth was assessed following 24 to 48 h  
541 of incubation on Mueller-Hinton agar (Becton, Dickinson, MD, USA). The *B. multivorans* ATCC  
542 17616 strain was included as a positive control, while *P. aeruginosa* ATCC 27853 and *E. coli*  
543 ATCC 25922 were used as quality controls.

544

545 **Sequencing and Quality Control.** *B. multivorans* isolates were whole-genome sequenced on  
546 the MiSeq and NextSeq Illumina platforms. The number of bases sequenced per isolate ranged  
547 from 213 to 2,262 million bases, and the median was 1,002 million bases. Trimmomatic v. 0.33  
548 was used to remove adapters and quality trim the sequencing reads from each isolate  
549 (parameter settings: PE -phred33 ILLUMINACLIP:adapters.fa:2:30:10 LEADING:5 TRAILING:5  
550 SLIDINGWINDOW:4:25) [47]. Sequencing reads with guanine homopolymers longer than ten  
551 bases were trimmed with cutadapt v. 1.9.1 (parameter settings: -a "G{10}") [48]. Reads below  
552 100 bases were removed using Trimmomatic v. 0.33 (parameter settings: PE -phred33  
553 MINLENGTH:100). The resulting quality-controlled sequencing reads yielded a median read  
554 depth per position of 117X (range 32-276X).

555

556 **De novo and Reference Mapping Assembly.** Each of the isolates was *de novo* assembled  
557 using the CLC Genomics Workbench v. 8.0.1 (Aarhus, Denmark). Contigs with a scaffolding  
558 depth lower than 10X and/or with a size smaller than 1 Kb were removed from further analyses.  
559 Isolate CF170-3b, which was sequenced with 250 bp-long paired-end reads, yielded the best  
560 assembly metrics in 26 contigs with lengths ranging from 1,010 to 1,243,078 bases and an N50  
561 of 654,231. The final assembly length of the CF170-3b isolate was of 6,444,123 bp. These  
562 contigs were annotated at the RAST server using the native gene caller and Classic RAST as  
563 the annotation scheme [47]. Further, this genome was functionally annotated with blast2go v  
564 4.1.9 [49] including blastx v. 2.6.0+ [50]. Statistical results from the functional enrichment  
565 analysis were Bonferroni corrected for multiple testing using the number of multiply-mutated  
566 genes (P-value/62). The contigs of the CF170-3b genome were used as the reference for  
567 mapping assembly of each remaining isolate. We performed three different reference-mapping  
568 assemblies including BWA v 0.7.12 [51], LAST v 284v [52] and novoalign v 2.08.03 (Novocraft  
569 Technologies).

570

571 **Single Nucleotide Polymorphism (SNP) and indel Calling.** SAMtools and BCFtools v 0.1.19  
572 were used to produce the initial set of variants [53]. We implemented a method previously  
573 described to detect SNPs among the 111 isolates [25, 54]. First, 1,892 high-confidence  
574 polymorphic positions were identified using the following criteria: 1) variant Phred quality score  
575 of  $\geq 30$  and 2) variants must be found at least 150 bp away from either the edge of the reference  
576 contig or an indel. Second, we reviewed each high-confidence polymorphic position in each  
577 isolate with a relaxed Phred score threshold of 25. Support for either the reference or the SNP  
578 call was verified with a multi-hypothesis correction which required that at least 80% of the  
579 sequencing reads endorsed the SNP or the reference. If the data did not support either base,  
580 then the position was called as an ambiguous base ('N'). The ambiguous call rate was lower  
581 than 0.01%.

582

583 Candidate indels detected by BWA and SAMtools were examined by realigning mapped and  
584 unmapped sequencing reads to the indel regions using Dindel v. 1.01 [55]. High-confidence  
585 indel positions were defined as sites with: 1) variant Phred quality score of  $\geq 35$ ; 2) at least two  
586 forward and two reverse reads; and 3) sequencing coverage  $\geq 10$ . These indel positions were  
587 reviewed in each isolate. The final indel call required a Phred quality score  $\geq 25$  and an allele  
588 frequency  $\geq 80\%$ . Ambiguous indel calls were defined as those where the allele frequency was  
589  $\leq 20\%$ .

590

591 **Population and Single Genome Sequencing Evaluation.** We performed bulk population  
592 sequencing on the post-transplant specimen to confirm that our isolate sampling depth  
593 appropriately represented the real *B. multivorans* population diversity (S9 Fig). The sequencing  
594 reads from each of the ten isolates from the post-transplant sample were rarified to 1/10<sup>th</sup> of the  
595 number of sequencing reads produced by the population sequencing experiment. These reads  
596 were combined in corresponding paired-end fasta files. Next, population and single isolate  
597 sequencing reads were mapped to the *de novo* assembled genome of the CF170-3b isolate  
598 using BWA. Mutation allele frequencies for each experiment were estimated as previously  
599 described by Lieberman *et al.* [54].

600

601 **Phylogenetic, Population Structure, Coalescent and Recombination Analyses.** Using the  
602 1,892 SNPs, we created a genome-wide alignment to reconstruct the phylogenetic relationships  
603 among the 111 isolates. The phylogeny was calculated using MrBayes v. 3.2.6 [56]. The

604 nucleotide substitution model that best fit our data was the General Time Reversible (GTR) with  
605 gamma-distributed rate variation across sites ( $\text{LnL}=-13,152.7810$ ,  $\text{AIC}= 26,832.1306$ ) as  
606 calculated with jModelTest v. 2.1.10 [57]. The Bayesian analysis was run through four different  
607 chains of 1 million Markov Chain Monte Carlo (MCMC) generations sampled every 100 MCMC  
608 generations and the burn-in period was of 250,000 MCMC generations. The final average  
609 standard deviation of split frequencies was of  $7.3 \times 10^{-3}$ , and the potential scale reduction factor  
610 (PSRF) of the substitution model parameters ranged from  $1 - 6.66 \times 10^{-5}$  to  $1 + 4.83 \times 10^{-4}$ . The  
611 phylogeny was rooted with *B. multivorans* ATCC 17616 [58]. The network-based phylogenetic  
612 analysis was performed using SplitsTree v 4.14.4 [59]. We employed the Jukes-Cantor distance  
613 matrix to implement the neighbor-net Network (Fit=99.804).

614

615 The variance among the 111 isolates, including SNPs and indels, was employed to investigate  
616 the population structure using the Structure software v 2.3.4 [60]. Structure employs a Bayesian  
617 algorithm to detect the number of ancestral populations (K), also known as clusters, which  
618 describe the variance and covariance observed in a test population. The number of clusters  
619 ranging from 1-10 was tested in triplicates through 1 million MCMC generations sampled every  
620 1,000 MCMC generations and a burn-in period of 250,000 MCMC generations. We used the  
621 correlated allele frequencies model, and admixture was allowed in these analyses. We plotted  
622 the estimated  $\ln$  probability of data for the tested levels of K, and identified the smallest stable K  
623 as the optimum value since it maximized the global likelihood of the data (S10 Fig) [61]. The  
624 estimated  $\ln$  probability of data plateaus at K=3, where the variance of  $\ln$  likelihood ranges from  
625 2,343.0 to 2,353.1. Assuming three ancestral populations, the isolates were classified into five  
626 different groups according to their ancestry. Isolates whose ancestry is attributed exclusively  
627 (>90%) to either ancestral population one, two, or three are grouped in group red (R), (B), or  
628 (G), respectively. Group RB includes isolates with admixed ancestry from clusters one and two  
629 (at least 10% of both cluster one and two, and less than 10% of cluster three). Isolates whose  
630 ancestral composition is made up from a combination of all three clusters (at least 10% of each  
631 cluster) are in group RBG.

632

633 We used BEAST v. 1.8.4 to implement a Bayesian approach to inferring the time to the most  
634 recent common ancestor (tMRCA) for the entire population and each group individually [62].  
635 Next, we employed the GTR nucleotide substitution model, and estimated the nucleotide  
636 substitution frequencies with MEGA7 using the Maximum Likelihood Estimate of the Substitution  
637 Matrix tool ([AC] = 0.0091, [AG] = 0.4281, [AT] = 0.0016, [CG] = 0.0260, [GT] = 0.0061, and

638 [CT] = 0.5290). Preliminary analyses consisting of duplicate 10 million generations and a 10%  
639 burn-in were used to estimate the appropriate molecular clock and demographic models. We  
640 tested the Bayesian skygrid, constant size and the exponential, logarithmic and expansion  
641 growth population size models using three different molecular clock models (strict and the  
642 lognormal and exponential uncorrelated relaxed clocks). The exponential relaxed uncorrelated  
643 molecular clock and the Bayesian skygrid model was inferred the most appropriate given our  
644 data ([AIC] = 26,228.421) [63]. The final analysis was run in duplicate for 1 billion MCMC  
645 generations sampled every 1,000 MCMC generation, and the burn-in period was set at 20% of  
646 the MCMC generations.

647

648 Population genetic tests and detection of recombination events in each contig were performed  
649 with DnaSP v. 5.10.01 [64].

650

651 **SNP to Phenotype Association.** We tested the null hypothesis that the presence or absence  
652 of each of the 1,892 SNPs, summarized in 150 distinct mutational profiles, is equally likely found  
653 in antibiotic resistant isolates using Fisher's exact test. These tests were conducted for each  
654 examined antibiotic at six different MIC resistance thresholds ( $\leq 16, 32, 64, 128, 256$  and  $\leq 512$   
655 MIC). For each test, we created a contingency table reflecting the distribution of each mutation  
656 profile in isolates with lower and greater MIC than each resistance threshold.  $P$  values were  
657 adjusted based on the total number of tests (number of mutational profiles), and only  
658 associations with a  $P$  value  $< 3.36 \times 10^{-4}$  ( $0.05 / 150$ ) were considered significant to control for  
659 multiple testing. Next, we simulated gains or losses of these mutational events following a  
660 continuous-time Markov chain along a ClonalFrameML v. 1.0-19 phylogeny as implemented in  
661 GLOOME v. 01.266 using the default parameters [65, 66]. We defined independent mutational  
662 events as those with a probability greater than 0.95 and to control for population structure, we  
663 required multiple independent mutational events in at least two STRUCTURE-defined groups.

664

665 ***In silico* mutation impact prediction.** To predict the potential impact of non-synonymous  
666 SNPs on the biological function of a protein, we employed PROVEAN v. 1.1.3 [67]. These  
667 calculations were performed on the GPC supercomputer at the SciNet HPC Consortium [68].

668

669

670

671 **Acknowledgements**

672 This research was funded by an Emerging Team Grant awarded to D.S.G from the Canadian  
673 Institutes of Health Research (CIHR) and Cystic Fibrosis Canada (CMF108027). J.D.C. was  
674 supported by an Ontario Trillium Scholarship. S.T.C. was supported by an Ontario Graduate  
675 Scholarship. B.C. was supported by a CIHR Fellowship. **We would like to thank Dr. Tami**  
676 **Lieberman for her assistance with the estimation of the dN/dS rates.**

## 677 References

- 678 1. Vandamme P, Dawyndt P. Classification and identification of the *Burkholderia cepacia*  
679 complex: Past, present and future. *Syst Appl Microbiol.* 2011;34(2):87-95. Epub 2011/01/25.  
680 doi: 10.1016/j.syapm.2010.10.002. PubMed PMID: 21257278.
- 681 2. De Smet B, Mayo M, Peeters C, Zlosnik JE, Spilker T, Hird TJ, et al. *Burkholderia stagnalis*  
682 sp. nov. and *Burkholderia territorii* sp. nov., two novel *Burkholderia cepacia* complex species  
683 from environmental and human sources. *Int J Syst Evol Microbiol.* 2015;65(7):2265-71.  
684 Epub 2015/04/16. doi: 10.1099/ijss.0.000251. PubMed PMID: 25872960.
- 685 3. Courtney JM, Bradley J, McCaughan J, O'Connor TM, Shortt C, Bredin CP, et al. Predictors  
686 of mortality in adults with cystic fibrosis. *Pediatr Pulmonol.* 2007;42(6):525-32. Epub  
687 2007/05/01. doi: 10.1002/ppul.20619. PubMed PMID: 17469153.
- 688 4. Stephenson AL, Sykes J, Berthiaume Y, Singer LG, Aaron SD, Whitmore GA, et al. Clinical  
689 and demographic factors associated with post-lung transplantation survival in individuals  
690 with cystic fibrosis. *J Heart Lung Transplant.* 2015;34(9):1139-45. Epub 2015/06/20. doi:  
691 10.1016/j.healun.2015.05.003. PubMed PMID: 26087666.
- 692 5. Drevinek P, Mahenthiralingam E. *Burkholderia cenocepacia* in cystic fibrosis: epidemiology  
693 and molecular mechanisms of virulence. *Clin Microbiol Infect.* 2010;16(7):821-30. doi:  
694 10.1111/j.1469-0691.2010.03237.x. PubMed PMID: 20880411.
- 695 6. Lipuma JJ. The changing microbial epidemiology in cystic fibrosis. *Clin Microbiol Rev.*  
696 2010;23(2):299-323. Epub 2010/04/09. doi: 10.1128/CMR.00068-09. PubMed PMID:  
697 20375354; PubMed Central PMCID: PMC2863368.
- 698 7. Lipuma JJ. Update on the *Burkholderia cepacia* complex. *Current opinion in Pulmonary  
699 Medicine.* 2005;11(6):528-33. Epub 2005/10/12. doi: 00063198-200511000-00010 [pii].  
700 PubMed PMID: 16217180.
- 701 8. Jones AM, Dodd ME, Govan JR, Barcus V, Doherty CJ, Morris J, et al. *Burkholderia  
702 cenocepacia* and *Burkholderia multivorans*: influence on survival in cystic fibrosis. *Thorax.*  
703 2004;59(11):948-51. Epub 2004/11/02. doi: 59/11/948 [pii]  
704 10.1136/thx.2003.017210. PubMed PMID: 15516469; PubMed Central PMCID: PMC1746874.
- 705 9. Leitao JH, Sousa SA, Ferreira AS, Ramos CG, Silva IN, Moreira LM. Pathogenicity,  
706 virulence factors, and strategies to fight against *Burkholderia cepacia* complex pathogens  
707 and related species. *Appl Microbiol Biotechnol.* 2010;87(1):31-40. Epub 2010/04/15. doi:  
708 10.1007/s00253-010-2528-0. PubMed PMID: 20390415.
- 709 10. Zlosnik JE, Zhou G, Brant R, Henry DA, Hird TJ, Mahenthiralingam E, et al. *Burkholderia*  
710 species infections in patients with cystic fibrosis in British Columbia, Canada. 30 years'

- 711       experience. *Ann Am Thorac Soc.* 2015;12(1):70-8. Epub 2014/12/05. doi:  
712       10.1513/AnnalsATS.201408-395OC. PubMed PMID: 25474359.
- 713       11. Rhodes KA, Schweizer HP. Antibiotic resistance in *Burkholderia* species. *Drug Resist  
714       Updat.* 2016;28:82-90. Epub 2016/09/14. doi: 10.1016/j.drup.2016.07.003. PubMed PMID:  
715       27620956; PubMed Central PMCID: PMCPMC5022785.
- 716       12. Price AL, Spencer CC, Donnelly P. Progress and promise in understanding the genetic  
717       basis of common diseases. *Proc Biol Sci.* 2015;282(1821):20151684. doi:  
718       10.1098/rspb.2015.1684. PubMed PMID: 26702037; PubMed Central PMCID:  
719       PMCPMC4707742.
- 720       13. McCarthy MI, Abecasis GR, Cardon LR, Goldstein DB, Little J, Ioannidis JP, et al. Genome-  
721       wide association studies for complex traits: consensus, uncertainty and challenges. *Nat Rev  
722       Genet.* 2008;9(5):356-69. doi: 10.1038/nrg2344. PubMed PMID: 18398418.
- 723       14. Power RA, Parkhill J, de Oliveira T. Microbial genome-wide association studies: lessons  
724       from human GWAS. *Nat Rev Genet.* 2017;18(1):41-50. doi: 10.1038/nrg.2016.132. PubMed  
725       PMID: 27840430.
- 726       15. Farhat MR, Shapiro BJ, Kieser KJ, Sultana R, Jacobson KR, Victor TC, et al. Genomic  
727       analysis identifies targets of convergent positive selection in drug-resistant *Mycobacterium*  
728       tuberculosis. *Nat Genet.* 2013;45(10):1183-9. doi: 10.1038/ng.2747. PubMed PMID:  
729       23995135; PubMed Central PMCID: PMCPMC3887553.
- 730       16. Chewapreecha C, Harris SR, Croucher NJ, Turner C, Marttinen P, Cheng L, et al. Dense  
731       genomic sampling identifies highways of pneumococcal recombination. *Nat Genet.*  
732       2014;46(3):305-9. Epub 2014/02/11. doi: 10.1038/ng.2895. PubMed PMID: 24509479;  
733       PubMed Central PMCID: PMCPMC3970364.
- 734       17. Chewapreecha C, Marttinen P, Croucher NJ, Salter SJ, Harris SR, Mather AE, et al.  
735       Comprehensive identification of single nucleotide polymorphisms associated with beta-  
736       lactam resistance within pneumococcal mosaic genes. *PLoS Genet.* 2014;10(8):e1004547.  
737       doi: 10.1371/journal.pgen.1004547. PubMed PMID: 25101644; PubMed Central PMCID:  
738       PMCPMC4125147.
- 739       18. Chen PE, Shapiro BJ. The advent of genome-wide association studies for bacteria. *Curr  
740       Opin Microbiol.* 2015;25:17-24. doi: 10.1016/j.mib.2015.03.002. PubMed PMID: 25835153.
- 741       19. Sheppard SK, Didelot X, Meric G, Torralbo A, Jolley KA, Kelly DJ, et al. Genome-wide  
742       association study identifies vitamin B5 biosynthesis as a host specificity factor in  
743       *Campylobacter*. *Proc Natl Acad Sci U S A.* 2013;110(29):11923-7. doi:

- 744 10.1073/pnas.1305559110. PubMed PMID: 23818615; PubMed Central PMCID:  
745 PMCPMC3718156.
- 746 20. Chaston JM, Newell PD, Douglas AE. Metagenome-wide association of microbial  
747 determinants of host phenotype in *Drosophila melanogaster*. MBio. 2014;5(5):e01631-14.  
748 doi: 10.1128/mBio.01631-14. PubMed PMID: 25271286; PubMed Central PMCID:  
749 PMCPMC4196228.
- 750 21. Earle SG, Wu CH, Charlesworth J, Stoesser N, Gordon NC, Walker TM, et al. Identifying  
751 lineage effects when controlling for population structure improves power in bacterial  
752 association studies. Nat Microbiol. 2016;1:16041. doi: 10.1038/nmicrobiol.2016.41. PubMed  
753 PMID: 27572646; PubMed Central PMCID: PMCPMC5049680.
- 754 22. Didelot X, Maiden MC. Impact of recombination on bacterial evolution. Trends Microbiol.  
755 2010;18(7):315-22. doi: 10.1016/j.tim.2010.04.002. PubMed PMID: 20452218; PubMed  
756 Central PMCID: PMCPMC3985120.
- 757 23. Hughes D, Andersson DI. Evolutionary consequences of drug resistance: shared principles  
758 across diverse targets and organisms. Nat Rev Genet. 2015;16(8):459-71. doi:  
759 10.1038/nrg3922. PubMed PMID: 26149714.
- 760 24. Jolley KA, Maiden MC. BIGSdb: Scalable analysis of bacterial genome variation at the  
761 population level. BMC Bioinformatics. 2010;11:595. doi: 10.1186/1471-2105-11-595.  
762 PubMed PMID: 21143983; PubMed Central PMCID: PMCPMC3004885.
- 763 25. Diaz Caballero J, Clark ST, Coburn B, Zhang Y, Wang PW, Donaldson SL, et al. Selective  
764 Sweeps and Parallel Pathoadaptation Drive *Pseudomonas aeruginosa* Evolution in the  
765 Cystic Fibrosis Lung. MBio. 2015;6(5):e00981-15. doi: 10.1128/mBio.00981-15. PubMed  
766 PMID: 26330513; PubMed Central PMCID: PMCPMC4556809.
- 767 26. McVean G. The structure of linkage disequilibrium around a selective sweep. Genetics.  
768 2007;175(3):1395-406. doi: 10.1534/genetics.106.062828. PubMed PMID: 17194788;  
769 PubMed Central PMCID: PMCPMC1840056.
- 770 27. Kalinowski ST. The computer program STRUCTURE does not reliably identify the main  
771 genetic clusters within species: simulations and implications for human population structure.  
772 Heredity (Edinb). 2011;106(4):625-32. doi: 10.1038/hdy.2010.95. PubMed PMID: 20683484;  
773 PubMed Central PMCID: PMCPMC3183908.
- 774 28. Hwang J, Kim HS. Cell Wall Recycling-Linked Coregulation of AmpC and PenB beta-  
775 Lactamases through ampD Mutations in *Burkholderia cenocepacia*. Antimicrob Agents  
776 Chemother. 2015;59(12):7602-10. doi: 10.1128/AAC.01068-15. PubMed PMID: 26416862;  
777 PubMed Central PMCID: PMCPMC4649219.

- 778 29. Kong KF, Schneper L, Mathee K. Beta-lactam antibiotics: from antibiosis to resistance and  
779 bacteriology. *APMIS*. 2010;118(1):1-36. doi: 10.1111/j.1600-0463.2009.02563.x. PubMed  
780 PMID: 20041868; PubMed Central PMCID: PMCPMC2894812.
- 781 30. Wood TE, Burke JM, Rieseberg LH. Parallel genotypic adaptation: when evolution repeats  
782 itself. *Genetica*. 2005;123(1-2):157-70. PubMed PMID: 15881688; PubMed Central PMCID:  
783 PMCPMC2442917.
- 784 31. Westfall LW, Carty NL, Layland N, Kuan P, Colmer-Hamood JA, Hamood AN. *mvaT*  
785 mutation modifies the expression of the *Pseudomonas aeruginosa* multidrug efflux operon  
786 *mexEF-oprN*. *FEMS Microbiol Lett*. 2006;255(2):247-54. doi: 10.1111/j.1574-  
787 6968.2005.00075.x. PubMed PMID: 16448502.
- 788 32. da Silva PE, Von Groll A, Martin A, Palomino JC. Efflux as a mechanism for drug resistance  
789 in *Mycobacterium tuberculosis*. *FEMS Immunol Med Microbiol*. 2011;63(1):1-9. doi:  
790 10.1111/j.1574-695X.2011.00831.x. PubMed PMID: 21668514.
- 791 33. Coyne S, Courvalin P, Perichon B. Efflux-mediated antibiotic resistance in *Acinetobacter*  
792 spp. *Antimicrob Agents Chemother*. 2011;55(3):947-53. doi: 10.1128/AAC.01388-10.  
793 PubMed PMID: 21173183; PubMed Central PMCID: PMCPMC3067115.
- 794 34. Stephenson K, Hoch JA. Two-component and phosphorelay signal-transduction systems as  
795 therapeutic targets. *Curr Opin Pharmacol*. 2002;2(5):507-12. Epub 2002/09/27. PubMed  
796 PMID: 12324251.
- 797 35. Potvin E, Sanschagrin F, Levesque RC. Sigma factors in *Pseudomonas aeruginosa*. *FEMS*  
798 *Microbiol Rev*. 2008;32(1):38-55. doi: 10.1111/j.1574-6976.2007.00092.x. PubMed PMID:  
799 18070067.
- 800 36. Barton NH. Richard Hudson and Norman Kaplan on the Coalescent Process. *Genetics*.  
801 2016;202(3):865-6. doi: 10.1534/genetics.116.187542. PubMed PMID: 26953263; PubMed  
802 Central PMCID: PMCPMC4788121.
- 803 37. Folkesson A, Jelsbak L, Yang L, Johansen HK, Ciofu O, Hoiby N, et al. Adaptation of  
804 *Pseudomonas aeruginosa* to the cystic fibrosis airway: an evolutionary perspective. *Nat Rev*  
805 *Microbiol*. 2012;10(12):841-51. Epub 2012/11/14. doi: 10.1038/nrmicro2907. PubMed PMID:  
806 23147702.
- 807 38. Blair JM, Webber MA, Baylay AJ, Ogbolu DO, Piddock LJ. Molecular mechanisms of  
808 antibiotic resistance. *Nat Rev Microbiol*. 2015;13(1):42-51. doi: 10.1038/nrmicro3380.  
809 PubMed PMID: 25435309.
- 810 39. Garcia-Solache M, Lebreton F, McLaughlin RE, Whiteaker JD, Gilmore MS, Rice LB.  
811 Homologous Recombination within Large Chromosomal Regions Facilitates Acquisition of

- 812 beta-Lactam and Vancomycin Resistance in *Enterococcus faecium*. *Antimicrob Agents*  
813 *Chemother*. 2016;60(10):5777-86. doi: 10.1128/AAC.00488-16. PubMed PMID: 27431230;  
814 PubMed Central PMCID: PMCPMC5038250.
- 815 40. Aubert D, Naas T, Nordmann P. Integrase-mediated recombination of the *veb1* gene  
816 cassette encoding an extended-spectrum beta-lactamase. *PLoS One*. 2012;7(12):e51602.  
817 doi: 10.1371/journal.pone.0051602. PubMed PMID: 23251590; PubMed Central PMCID:  
818 PMCPMC3518468.
- 819 41. Marvig RL, Sommer LM, Molin S, Johansen HK. Convergent evolution and adaptation of  
820 *Pseudomonas aeruginosa* within patients with cystic fibrosis. *Nat Genet*. 2015;47(1):57-64.  
821 doi: 10.1038/ng.3148. PubMed PMID: 25401299.
- 822 42. Sokurenko EV, Hasty DL, Dykhuizen DE. Pathoadaptive mutations: gene loss and variation  
823 in bacterial pathogens. *Trends Microbiol*. 1999;7(5):191-5. PubMed PMID: 10354593.
- 824 43. Arellano-Reynoso B, Lapaque N, Salcedo S, Briones G, Ciocchini AE, Ugalde R, et al.  
825 Cyclic beta-1,2-glucan is a *Brucella* virulence factor required for intracellular survival. *Nat*  
826 *Immunol*. 2005;6(6):618-25. doi: 10.1038/ni1202. PubMed PMID: 15880113.
- 827 44. Clark ST, Diaz Caballero J, Cheang M, Coburn B, Wang PW, Donaldson SL, et al.  
828 Phenotypic diversity within a *Pseudomonas aeruginosa* population infecting an adult with  
829 cystic fibrosis. *Sci Rep*. 2015;5:10932. doi: 10.1038/srep10932. PubMed PMID: 26047320;  
830 PubMed Central PMCID: PMCPMC4456944.
- 831 45. Spilker T, Baldwin A, Bumford A, Dowson CG, Mahenthiralingam E, LiPuma JJ. Expanded  
832 multilocus sequence typing for *burkholderia* species. *J Clin Microbiol*. 2009;47(8):2607-10.  
833 doi: 10.1128/JCM.00770-09. PubMed PMID: 19494070; PubMed Central PMCID:  
834 PMCPMC2725695.
- 835 46. CLSI. Methods for Dilution Antimicrobial Susceptibility Tests for Bacteria That Grow  
836 Aerobically; Approved Standard M07-A9. Wayne, PA: Clinical and Laboratory Standards  
837 Institute; 2012.
- 838 47. Bolger AM, Lohse M, Usadel B. Trimmomatic: a flexible trimmer for Illumina sequence data.  
839 *Bioinformatics*. 2014;30(15):2114-20. doi: 10.1093/bioinformatics/btu170. PubMed PMID:  
840 WOS:000340049100004.
- 841 48. Martin M. Cutadapt removes adapter sequences from high-throughput sequencing reads.  
842 2011. 2011;17(1). doi: 10.14806/ej.17.1.200  
843 pp. 10-12.
- 844 49. Gotz S, Garcia-Gomez JM, Terol J, Williams TD, Nagaraj SH, Nueda MJ, et al. High-  
845 throughput functional annotation and data mining with the Blast2GO suite. *Nucleic Acids*

- 846 Res. 2008;36(10):3420-35. Epub 2008/05/01. doi: 10.1093/nar/gkn176. PubMed PMID:  
847 18445632; PubMed Central PMCID: PMCPMC2425479.
- 848 50. Altschul SF, Madden TL, Schaffer AA, Zhang J, Zhang Z, Miller W, et al. Gapped BLAST  
849 and PSI-BLAST: a new generation of protein database search programs. Nucleic Acids Res.  
850 1997;25(17):3389-402. Epub 1997/09/01. PubMed PMID: 9254694; PubMed Central  
851 PMCID: PMCPMC146917.
- 852 51. Li H, Durbin R. Fast and accurate short read alignment with Burrows-Wheeler transform.  
853 Bioinformatics. 2009;25(14):1754-60. doi: 10.1093/bioinformatics/btp324. PubMed PMID:  
854 19451168; PubMed Central PMCID: PMCPMC2705234.
- 855 52. Shrestha AM, Frith MC. An approximate Bayesian approach for mapping paired-end DNA  
856 reads to a reference genome. Bioinformatics. 2013;29(8):965-72. doi:  
857 10.1093/bioinformatics/btt073. PubMed PMID: 23413433; PubMed Central PMCID:  
858 PMCPMC3624798.
- 859 53. Li H, Handsaker B, Wysoker A, Fennell T, Ruan J, Homer N, et al. The Sequence  
860 Alignment/Map format and SAMtools. Bioinformatics. 2009;25(16):2078-9. doi:  
861 10.1093/bioinformatics/btp352. PubMed PMID: 19505943; PubMed Central PMCID:  
862 PMCPMC2723002.
- 863 54. Lieberman TD, Michel JB, Aingaran M, Potter-Bynoe G, Roux D, Davis MR, Jr., et al.  
864 Parallel bacterial evolution within multiple patients identifies candidate pathogenicity genes.  
865 Nat Genet. 2011;43(12):1275-80. doi: 10.1038/ng.997. PubMed PMID: 22081229; PubMed  
866 Central PMCID: PMCPMC3245322.
- 867 55. Albers CA, Lunter G, MacArthur DG, McVean G, Ouwehand WH, Durbin R. Dindel: accurate  
868 indel calls from short-read data. Genome Res. 2011;21(6):961-73. doi:  
869 10.1101/gr.112326.110. PubMed PMID: 20980555; PubMed Central PMCID:  
870 PMCPMC3106329.
- 871 56. Ronquist F, Huelsenbeck JP. MrBayes 3: Bayesian phylogenetic inference under mixed  
872 models. Bioinformatics. 2003;19(12):1572-4. PubMed PMID: 12912839.
- 873 57. Darriba D, Taboada GL, Doallo R, Posada D. jModelTest 2: more models, new heuristics  
874 and parallel computing. Nat Methods. 2012;9(8):772. doi: 10.1038/nmeth.2109. PubMed  
875 PMID: 22847109; PubMed Central PMCID: PMCPMC4594756.
- 876 58. Stanier RY, Palleroni NJ, Doudoroff M. The aerobic pseudomonads: a taxonomic study. J  
877 Gen Microbiol. 1966;43(2):159-271. doi: 10.1099/00221287-43-2-159. PubMed PMID:  
878 5963505.

- 879 59. Huson DH, Bryant D. Application of phylogenetic networks in evolutionary studies. *Mol Biol*  
880 *Evol.* 2006;23(2):254-67. doi: 10.1093/molbev/msj030. PubMed PMID: 16221896.
- 881 60. Pritchard JK, Stephens M, Donnelly P. Inference of population structure using multilocus  
882 genotype data. *Genetics*. 2000;155(2):945-59. PubMed PMID: 10835412; PubMed Central  
883 PMCID: PMCPMC1461096.
- 884 61. Porras-Hurtado L, Ruiz Y, Santos C, Phillips C, Carracedo A, Lareu MV. An overview of  
885 STRUCTURE: applications, parameter settings, and supporting software. *Front Genet*.  
886 2013;4:98. doi: 10.3389/fgene.2013.00098. PubMed PMID: 23755071; PubMed Central  
887 PMCID: PMCPMC3665925.
- 888 62. Drummond AJ, Suchard MA, Xie D, Rambaut A. Bayesian phylogenetics with BEAUTi and  
889 the BEAST 1.7. *Mol Biol Evol*. 2012;29(8):1969-73. doi: 10.1093/molbev/mss075. PubMed  
890 PMID: 22367748; PubMed Central PMCID: PMCPMC3408070.
- 891 63. Gill MS, Lemey P, Faria NR, Rambaut A, Shapiro B, Suchard MA. Improving Bayesian  
892 population dynamics inference: a coalescent-based model for multiple loci. *Mol Biol Evol*.  
893 2013;30(3):713-24. doi: 10.1093/molbev/mss265. PubMed PMID: 23180580; PubMed  
894 Central PMCID: PMCPMC3563973.
- 895 64. Librado P, Rozas J. DnaSP v5: a software for comprehensive analysis of DNA  
896 polymorphism data. *Bioinformatics*. 2009;25(11):1451-2. doi: 10.1093/bioinformatics/btp187.  
897 PubMed PMID: 19346325.
- 898 65. Didelot X, Wilson DJ. ClonalFrameML: efficient inference of recombination in whole bacterial  
899 genomes. *PLoS Comput Biol*. 2015;11(2):e1004041. doi: 10.1371/journal.pcbi.1004041.  
900 PubMed PMID: 25675341; PubMed Central PMCID: PMCPMC4326465.
- 901 66. Cohen O, Ashkenazy H, Belinky F, Huchon D, Pupko T. GLOOME: gain loss mapping  
902 engine. *Bioinformatics*. 2010;26(22):2914-5. doi: 10.1093/bioinformatics/btq549. PubMed  
903 PMID: 20876605.
- 904 67. Choi Y, Sims GE, Murphy S, Miller JR, Chan AP. Predicting the functional effect of amino  
905 acid substitutions and indels. *PLoS One*. 2012;7(10):e46688. doi:  
906 10.1371/journal.pone.0046688. PubMed PMID: 23056405; PubMed Central PMCID:  
907 PMCPMC3466303.
- 908 68. Chris L, Daniel G, Leslie G, Richard P, Neil B, Michael C, et al. SciNet: Lessons Learned  
909 from Building a Power-efficient Top-20 System and Data Centre. *Journal of Physics:*  
910 *Conference Series*. 2010;256(1):012026.
- 911 69. Krzywinski M, Schein J, Birol I, Connors J, Gascoyne R, Horsman D, et al. Circos: an  
912 information aesthetic for comparative genomics. *Genome Res*. 2009;19(9):1639-45. doi:

- 913 10.1101/gr.092759.109. PubMed PMID: 19541911; PubMed Central PMCID:  
914 PMCPMC2752132.
- 915 70. Letunic I, Bork P. Interactive tree of life (iTOL) v3: an online tool for the display and  
916 annotation of phylogenetic and other trees. Nucleic Acids Res. 2016;44(W1):W242-5. doi:  
917 10.1093/nar/gkw290. PubMed PMID: 27095192; PubMed Central PMCID:  
918 PMCPMC4987883.
- 919 71. Miller CA, McMichael J, Dang HX, Maher CA, Ding L, Ley TJ, et al. Visualizing tumor  
920 evolution with the fishplot package for R. BMC Genomics. 2016;17(1):880. doi:  
921 10.1186/s12864-016-3195-z. PubMed PMID: 27821060; PubMed Central PMCID:  
922 PMCPMC5100182.
- 923 72. Lieberman TD, Flett KB, Yelin I, Martin TR, McAdam AJ, Priebe GP, et al. Genetic variation  
924 of a bacterial pathogen within individuals with cystic fibrosis provides a record of selective  
925 pressures. Nat Genet. 2014;46(1):82-7. doi: 10.1038/ng.2848. PubMed PMID: 24316980;  
926 PubMed Central PMCID: PMCPMC3979468.
- 927 73. Stamatakis A. RAxML version 8: a tool for phylogenetic analysis and post-analysis of large  
928 phylogenies. Bioinformatics. 2014;30(9):1312-3. doi: 10.1093/bioinformatics/btu033.  
929 PubMed PMID: 24451623; PubMed Central PMCID: PMCPMC3998144.
- 930 74. Carrasco-Lopez C, Rojas-Altuve A, Zhang W, Hesek D, Lee M, Barbe S, et al. Crystal  
931 structures of bacterial peptidoglycan amidase AmpD and an unprecedented activation  
932 mechanism. J Biol Chem. 2011;286(36):31714-22. doi: 10.1074/jbc.M111.264366. PubMed  
933 PMID: 21775432; PubMed Central PMCID: PMCPMC3173140.
- 934

**Table 1. Parallel Pathoadapted Loci with Multiple Independent Mutations**

Locus	Encoded Protein	No. of SNPs/Indels	Probability <sup>a</sup>
BMUL_0641	Probable transcription regulator protein of MDR efflux pump cluster	7/0	1.65 X 10 <sup>-23</sup>
BCEN2424_5592 <sup>c</sup>	Glycosyltransferase 36	4/2	1.03 X 10 <sup>-19</sup>
BMUL_4010	NAD-glutamate dehydrogenase	5/0	6.48 X 10 <sup>-16</sup>
BMUL_0487	Hypothetical protein	5/0	6.48 X 10 <sup>-16</sup>
BMUL_4327	Porin	3/2	6.48 X 10 <sup>-16</sup>
BMUL_2790	N-acetyl-anhydromuranmyl-L-alanine amidase (AmpD)	5/0	6.48 X 10 <sup>-16</sup>
BMUL_1598	Amino acid adenylation domain-containing protein	4/0	4.06 X 10 <sup>-12</sup>
BMUL_0353	YD repeat-containing protein	3/1	4.06 X 10 <sup>-12</sup>
BMUL_0449	Preprotein translocase subunit (SecB)	4/0	4.06 X 10 <sup>-12</sup>
BMUL_2632	Chaperone protein (DnaJ)	4/0	4.06 X 10 <sup>-12</sup>
BMUL_4942	Signal transduction histidine kinase (CheA)	3/1	4.06 X 10 <sup>-12</sup>
BMUL_2775	UDP-N-acetylmuramate--L-alanyl-gamma-D-glutamyl-meso-diaminopimelate ligase	4/0	4.06 X 10 <sup>-12</sup>
BMUL_1444	Transcription termination factor (Rho)	4/0	4.06 X 10 <sup>-12</sup>
BMUL_0954	Glycoside hydrolase 15-like protein	4/0	4.06 X 10 <sup>-12</sup>
BMUL_4115	Outer membrane autotransporter	4/0	4.06 X 10 <sup>-12</sup>
BMUL_0250	50S ribosomal protein L4 (RplD)	3/0	2.55 X 10 <sup>-8</sup>
BMUL_5547	Conjugation protein (Trbl)	2/1	2.55 X 10 <sup>-8</sup>
BMUL_2931	TPR repeat-containing protein	3/0	2.55 X 10 <sup>-8</sup>
BMUL_3678	Integral membrane sensor signal transduction histidine kinase	3/0	2.55 X 10 <sup>-8</sup>
BMUL_3503	L-serine dehydratase 1	3/0	2.55 X 10 <sup>-8</sup>
BMUL_0690	RND efflux system outer membrane lipoprotein	2/1	2.55 X 10 <sup>-8</sup>
BMUL_0663	Alpha/beta hydrolase fold protein	3/0	2.55 X 10 <sup>-8</sup>
BMUL_0431	Histidine kinase	1/2	2.55 X 10 <sup>-8</sup>
BMUL_4510	Signal transduction histidine kinase (CheA)	2/1	2.55 X 10 <sup>-8</sup>
BMUL_1970	Major facilitator transporter	3/0	2.55 X 10 <sup>-8</sup>

BMUL_2008	Major facilitator transporter	2/1	2.55 X 10 <sup>-8</sup>
BMUL_2621	DNA mismatch repair protein (mutL)	1/2	2.55 X 10 <sup>-8</sup>
BMUL_4037	Esterase	3/0	2.55 X 10 <sup>-8</sup>
BMUL_3977	Metallophosphoesterase	2/1	2.55 X 10 <sup>-8</sup>
BMUL_4949	Aldehyde dehydrogenase	2/1	2.55 X 10 <sup>-8</sup>
BMUL_3951	Transcriptional regulator (AraC)	3/0	2.55 X 10 <sup>-8</sup>
BMUL_6019	Cytosine/purines uracil thiamine allantoin permease	2/1	2.55 X 10 <sup>-8</sup>
BMUL_0307	Amino acid carrier protein	3/0	2.55 X 10 <sup>-8</sup>
BMUL_5501	Cytochrome c oxidase subunit I	3/0	2.55 X 10 <sup>-8</sup>
BMUL_5087	Short-chain dehydrogenase/reductase SDR	3/0	2.55 X 10 <sup>-8</sup>
BMUL_4813	RNA polymerase sigma factor RpoD	3/0	2.55 X 10 <sup>-8</sup>
BMUL_3197	Beta-galactosidase	3/0	2.55 X 10 <sup>-8</sup>
BMUL_3212	Feruloyl-CoA synthase	3/0	2.55 X 10 <sup>-8</sup>
BMUL_3315	PA-phosphatase like phosphoesterase	1/2	2.55 X 10 <sup>-8</sup>
BMUL_3752	Peptidoglycan-binding (LysM)	3/0	2.55 X 10 <sup>-8</sup>
BMUL_3615	Aldehyde oxidase	3/0	2.55 X 10 <sup>-8</sup>
BMUL_1686	Ribonuclease R	3/0	2.55 X 10 <sup>-8</sup>
BMUL_4615 <sup>b</sup>	Amidophosphoribosyltransferase	3/0	2.55 X 10 <sup>-8</sup>
BMUL_4605	UTP-glucose-1-phosphate uridylyltransferase	3/0	2.55 X 10 <sup>-8</sup>
ABD05_14940 <sup>d</sup>	Isochorismatase	3/0	2.55 X 10 <sup>-8</sup>
BMUL_1431	GAF modulated sigma54 specific transcriptional regulator (Fis)	2/1	2.55 X 10 <sup>-8</sup>
BMUL_1377	N-acetyltransferase GCN5	3/0	2.55 X 10 <sup>-8</sup>
BMUL_0964	DNA polymerase III subunit alpha (DnaE)	3/0	2.55 X 10 <sup>-8</sup>
BMUL_0692	Carbohydrate kinase FGGY	2/1	2.55 X 10 <sup>-8</sup>
BMUL_0477	Error-prone DNA polymerase (DnaE2)	3/0	2.55 X 10 <sup>-8</sup>
BMUL_0443	Phosphoenolpyruvate-protein phosphotransferase	3/0	2.55 X 10 <sup>-8</sup>
BMUL_3068	Aldehyde dehydrogenase	3/0	2.55 X 10 <sup>-8</sup>
BMUL_4835	Hypothetical protein	2/1	2.55 X 10 <sup>-8</sup>
BMUL_1873	UvrD/REP helicase	3/0	2.55 X 10 <sup>-8</sup>
BMUL_2536	Hypothetical protein	3/0	2.55 X 10 <sup>-8</sup>
BMUL_2710	Outer membrane autotransporter	3/0	2.55 X 10 <sup>-8</sup>

BMUL_0123	Heavy metal translocating P-type ATPase	3/0	2.55 X 10 <sup>-8</sup>
BMUL_0116	Acyl-CoA dehydrogenase domain-containing protein	3/0	2.55 X 10 <sup>-8</sup>
BMUL_0075	Two component transcriptional regulator	2/1	2.55 X 10 <sup>-8</sup>
BMUL_4226	4-hydroxyphenylpyruvate dioxygenase	3/0	2.55 X 10 <sup>-8</sup>
BMUL_4749	Amino acid permease	2/1	2.55 X 10 <sup>-8</sup>
BMUL_4798	Integrase catalytic region	1/2	2.55 X 10 <sup>-8</sup>

<sup>a</sup> Calculated based on the probability of resampling with replacement any locus n times, given a genome size of N.  $P = (1/N)^{(n-1)}$ . We used (n – 1) since we are calculating the probability for any locus, rather than a specific locus.

<sup>b</sup> A mutation occurred in the intergenic region flanking the start codon of this locus.

<sup>c</sup> This locus is not found in ATCC 17616 The homolog with highest similarity is in *B. cenocepacia* DDS 22E-1

<sup>d</sup> This locus is not found in ATCC 17616 The homolog with highest similarity is in *B. cenocepacia* HI2424

**Table 2. Pairs of Mutations Occurring in the Same or in Neighboring Codons.**

Encoded Protein	Proximity
Regulatory protein GntR, HTH:GntR, C-terminal	Adjacent codon
Oligopeptide ABC transporter, periplasmic oligopeptide-binding protein (OppA)	2 codons away
Citrate-proton symporter	2 codons away
CDP-6-deoxy-delta-3,4-glucosene reductase-like	2 codons away
RNA polymerase sigma factor (RpoD) <sup>a</sup>	Same codon
Endo-1,4-beta-xylanase Z precursor <sup>b</sup>	Adjacent codon
Isoquinoline 1-oxidoreductase beta subunit <sup>b</sup>	2 codons away
LSU ribosomal protein L4p (L1e) <sup>b</sup>	Same codon
Chaperone protein (DnaJ) <sup>c</sup>	Adjacent codon
Probable transcription regulator protein of MDR efflux pump cluster <sup>d</sup>	2 codons away

a Loci additionally mutated 1 more time. Additional mutation is synonymous.

b Loci additionally mutated 1 more time. Additional mutation is non-synonymous.

c Locus additionally mutated 2 more times. All non-synonymous mutations.

d Locus additionally mutated 5 more times. All non-synonymous mutations.

937 **Figure Legends**

938

939 **Fig 1. Time course of *B. multivorans* infection in study patient CF170.** A total of 111 *B.*  
940 *multivorans* isolates from twelve collection times were used in this study (1 isolate from the  
941 initial infection, 10 isolates from each of 10 sputum samples collected during chronic infection,  
942 and 10 isolates from a sputum sample obtained during a post-transplant infection). Antibiotic  
943 treatment history during the chronic infection period is shown in the lower panel. Black bars  
944 indicate antibiotic administration, while hashed bars indicate intermittent exposure in that time  
945 block (only relevant prior to the start of chronic sampling). The method of antibiotic  
946 administration is shown as intravenous (iv), inhaled (inh), or oral (po).

947

948 **Fig 2. Genomic Characterization of 111 *B multivorans* isolates.** (A) Contigs (gray outer ring)  
949 of the *de novo* reference were arranged according to the three chromosomes of the complete  
950 genome of *B. multivorans* ATCC 17616. This genome was obtained from expectorated sputum  
951 collected in the third chronic infection sample. (B) Genome annotation according to RAST. (C)  
952 SNP count per 10 Kb as a function of their location in the contigs. Non-synonymous (orange),  
953 synonymous (yellow), putative regulatory (dark grey) and intergenic (light grey). (D) Indel (blue)  
954 count per 10 Kb. (E) Recombinogenic regions, as predicted by DnaSP Hudson-Kaplin four  
955 gamete test, are shown as red blocks. (F) Variants Associated with Antibiotic Resistance. From  
956 outermost to innermost ring: aztreonam and ceftazidime ( $\beta$ -lactam), amikacin and tobramycin  
957 (aminoglycoside), and ciprofloxacin (quinolone). This figure was prepared with circus v. 0.69  
958 [69].

959

960 **Fig 3. Population structure and antibiotic resistance profiles.** (A) Phylogenetic relationships  
961 of the 111 *B. multivorans* isolates were estimated employing a Bayesian approach based on  
962 genome-wide single nucleotide polymorphisms (SNPs). (B) Time of collection for each isolate.  
963 (C) Population structure analysis as assessed by Structure v2.3.4 with three expected ancestral  
964 subpopulations. Ancestral subpopulations are coded as red (R), blue (B), and green (G). (D)  
965 Isolates are grouped based on their ancestral composition. Group R, B, G, RB, and RBG are  
966 shaded in red, blue, green, purple, and grey respectively. (E) Antibiotic susceptibility for each  
967 isolate, the highest black circle represents the MIC ( $\mu$ g/mL), to the  $\beta$ -lactams: aztreonam and  
968 ceftazidime, the aminoglycosides: amikacin and tobramycin, and the quinolone: ciprofloxacin  
969 are shown as filled circles at six different concentration thresholds. This figure was elaborated at  
970 the interactive tree of life (iTOL) website v. 3 [70].

971

972 **Fig 4. Population genomics of the community over time.** Groups R, B, G, RB, and RBG are  
973 coloured in red, blue, green, purple, and grey respectively. (A) Frequency of each group over  
974 time. (B) The clonal graph was created with the assumption that RGB is the group of isolates  
975 resembling the ancestor of all the isolates, and RB is the group of isolates resembling the  
976 ancestor of group R and B. The distance between sample times is relative to the actual number  
977 of days between them. This plot was created using fishplot v. 0.3 [71].

978

979 **Fig 5. Distribution of pathoadaptive variants in recombinogenic regions of the genome.**  
980 (A) Distribution of the mutations associated with the tested antibiotics in the identified  
981 recombinogenic regions and in the rest of the genome (\*\* p < 0.0001, chi square test with  
982 multiple test correction). (B) Distribution of the mutations in multi-mutated loci in the identified  
983 recombinogenic regions and in the rest of the genome (\*\* p < 0.001, chi square test with  
984 multiple test correction).

985

986 **Supporting Information**

987

988 **S1 Fig. Sequencing coverage.** Whole genome sequencing of 111 isolates of *B. multivorans* in  
989 the Illumina platform. (A) Distribution of number of bases sequenced per isolate. (B) Distribution  
990 of median read depth per position.

991

992 **S2 Fig. Genetic diversity over time.** (A) Pairwise nucleotide differences between isolates  
993 collected from the same collection sample. Incident infection is not included since only one  
994 isolate was recovered from that time point. (B) Nucleotide differences between each isolate and  
995 the incident infection isolate.

996

997 **S3 Fig. Neighbor-Net phylogeny.** This network-based phylogeny was calculated in SplitsTree  
998 v. 4.14.4. Individual strain names at the tips of each branch have been replaced with pie charts  
999 indicating the distribution of dates during which the strains were sampled (indicated by the  
1000 circular legend).

1001

1002 **S4 Fig. Genetic diversity and selection analysis per group.** (A) Pairwise nucleotide  
1003 differences between isolates from the same group based on ancestry. (B)  $d_N/d_S$  per group  
1004 calculated including all SNPs and using only SNPs observed in multiple time points (MTP).  
1005  $dN/dS$  and the respective confidence intervals were calculated as described by Lieberman *et al.*  
1006 [72]. (C). Time to Most Recent Common Ancestry (tMRCA) as estimated using the BEAST  
1007 software for each group. The x axis represents the log of the years before the last sampling  
1008 time. The whiskers for each data point show the 95% high probability density intervals.

1009

1010 **S5 Fig. SNP positions with identical distribution of reference or alternative bases across**  
1011 **the strain collection are grouped into mutational profiles.** Here, “0”s and “1”s represent the  
1012 reference or alternative base, respectively, at each SNP position for each strain. SNP1 is the  
1013 only position where only Strain1 has a base alternative to the reference. Hence, mutational  
1014 profile 1, 1-0-0-0, comprises only one SNP. On the other hand, Strain4 is the only strain with a  
1015 variant base for positions SNP2 and SNP3. Therefore, mutational profile 2, 0-0-0-1, comprises  
1016 SNP2 and SNP3.

1017

1018 **S6 Fig. Mutational profiles associated with antibiotic resistance.** (A) Maximum Likelihood  
1019 phylogeny of 111 *B. multivorans* isolates was elaborated using RaxML v. 7.0.4 with a GTR +

1020 gamma model and 1,000 bootstraps [73]. Here, we show all mutation profiles associated with  
1021 antibiotic resistance prior to lineage control in black and with lineage control in orange. (B)  
1022 resistance to both  $\beta$ -lactams, (C) to amikacin only, (D) to both aminoglycosides, (E) to both  
1023 aminoglycosides and to ciprofloxacin, (F) and to ciprofloxacin only. A filled circle represents a  
1024 SNP call in the corresponding isolate compared to the reference.

1025

1026 **S7 Fig. Resistance levels at which genetic associations are statistically significant.**

1027 Mutational profiles were tested for association against six levels of antibiotic resistance (<16,  
1028 <32, <64, <128, <256 and <512 MIC) to five antibiotics (amikacin, tobramycin, aztreonam,  
1029 ceftazidime and ciprofloxacin). Black boxes show the levels of resistance at which the  
1030 mutational profiles were statistically significant including multi-testing correction. Associations to  
1031 ciprofloxacin antibiotic resistance are shown up to <128 MIC since no isolate had a MIC of 256  
1032 or greater in relation to that antibiotic.

1033

1034 **S8 Fig. Mutations in *ampD* locus.** (A) Distribution of the PROVEAN scores of all identified  
1035 non-synonymous substitutions highlighting SNPs in multi-mutated loci (yellow) and in the *ampD*  
1036 gene (red or blue if associated to  $\beta$ -lactam resistance). Red lines represent thresholds from  
1037 most specific (highest), to most sensitive (lowest) to determine if a mutation is deleterious to the  
1038 function of the gene in which it occurs. (B) Crystal structure of protein product of AmpD (PDB  
1039 ID:2Y2B, [74]) in complex with reaction products. Mutations found in our *B. multivorans*  
1040 population are colored in red or blue (mutations associated with  $\beta$ -lactam resistance).

1041

1042 **S9 Fig. Population and single isolate sequencing.** Sequencing reads from each isolate from  
1043 the post-transplant sample were rarified to 1/10th of the number of reads in the population  
1044 sequencing experiment; then they were combined so that the number of reads would be the  
1045 same for both experiments. Sequencing reads from the population and single isolate  
1046 experiments were mapped to the same reference as described above. Mutation allele  
1047 frequencies for both experiments were calculated using the quality thresholds described by  
1048 Lieberman *et al.* [54]. (A) Grey circles represent mutation allele frequencies in the deep  
1049 population sequencing experiment (y axis) versus in single isolate sequencing (x axis). The  
1050 dashed line represents the  $x=y$  function and the solid line is the best fit line taking into account  
1051 all data points ( $R^2=0.9928$ , 95% confidence interval= 0.9918-0.9937). Red circles represent  
1052 alleles found in the single isolate sequencing experiment but not in the deep sequencing one.

1053 Fixed mutations between the reference and all the post-transplant isolates are colored blue. (B)

1054 Proportion of false positives in the single isolate sequencing experiment.

1055

1056 **S10 Fig. Determining the number of ancestral populations that explain the variance and**

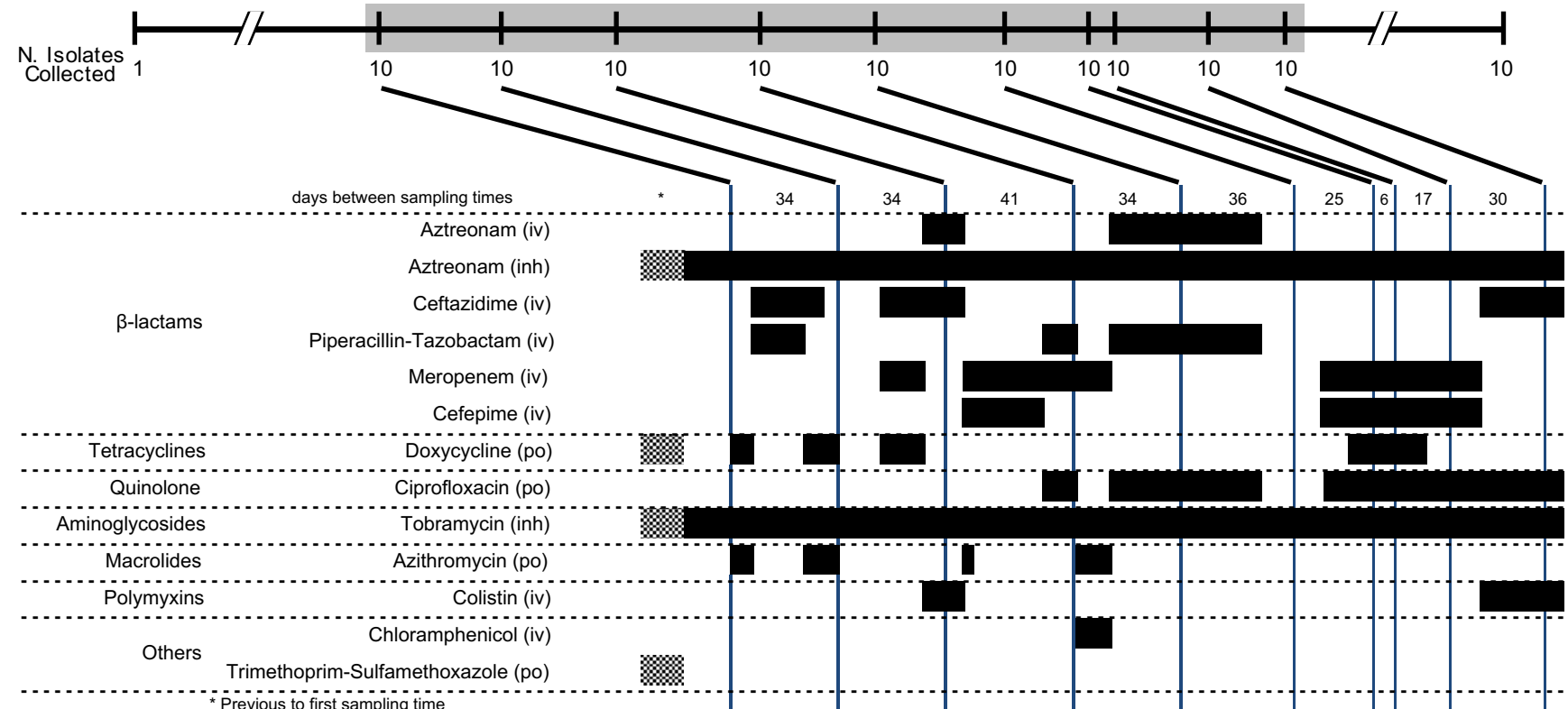
1057 **covariance in CF170 *B. multivorans* population.** (A) We ran three independent chains for

1058 each K between one and ten. The estimated ln probability of data plateaus at K=3 in all chains.

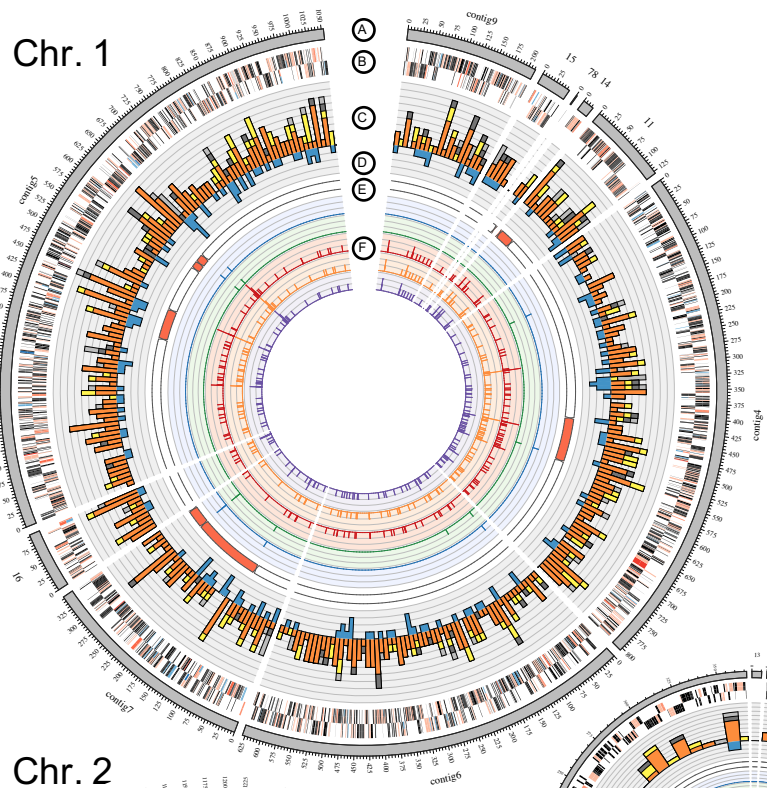
# Incident Infection 2005

## Chronic Infection 2011 - 2012

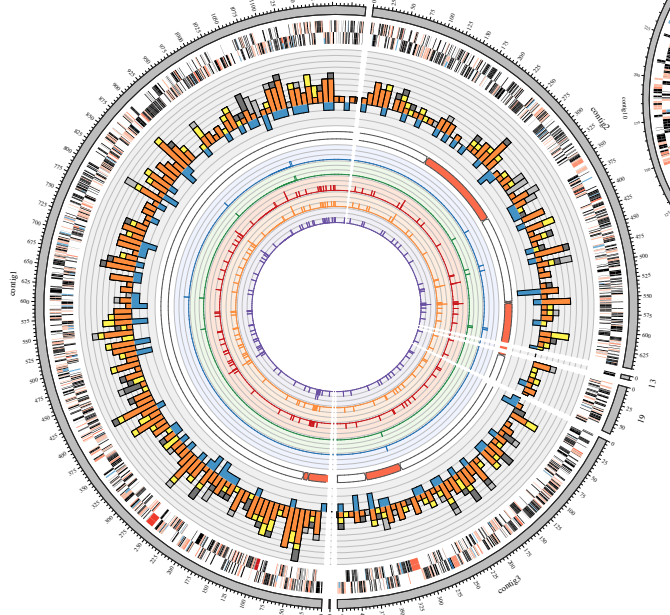
# Post-Transplant Infection 2015



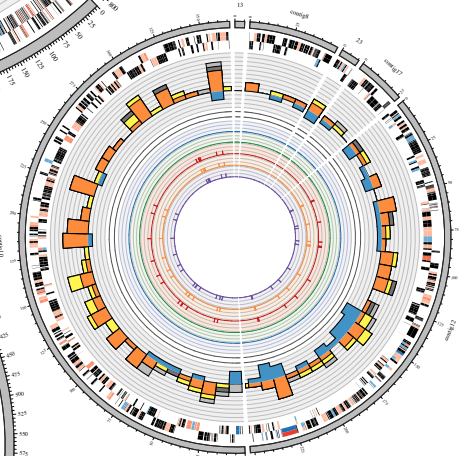
# Chr. 1



# Chr. 2

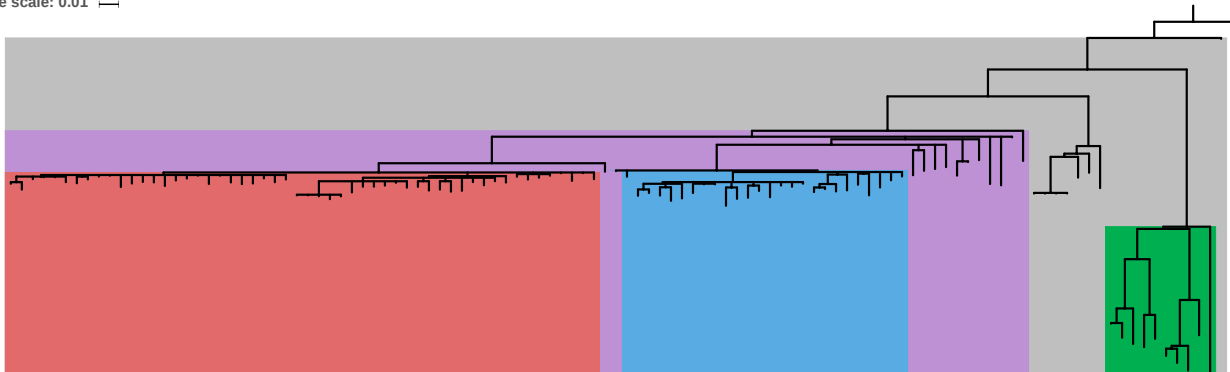


# Chr. 3

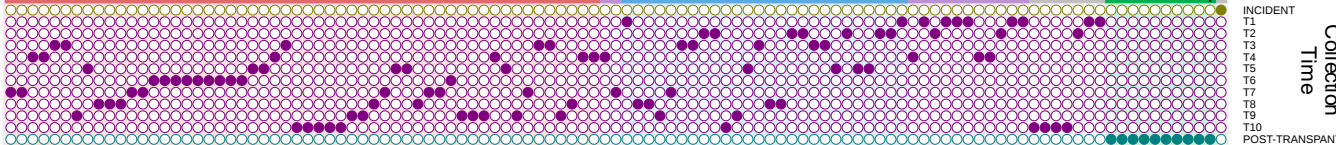


Tree scale: 0.01

A



B



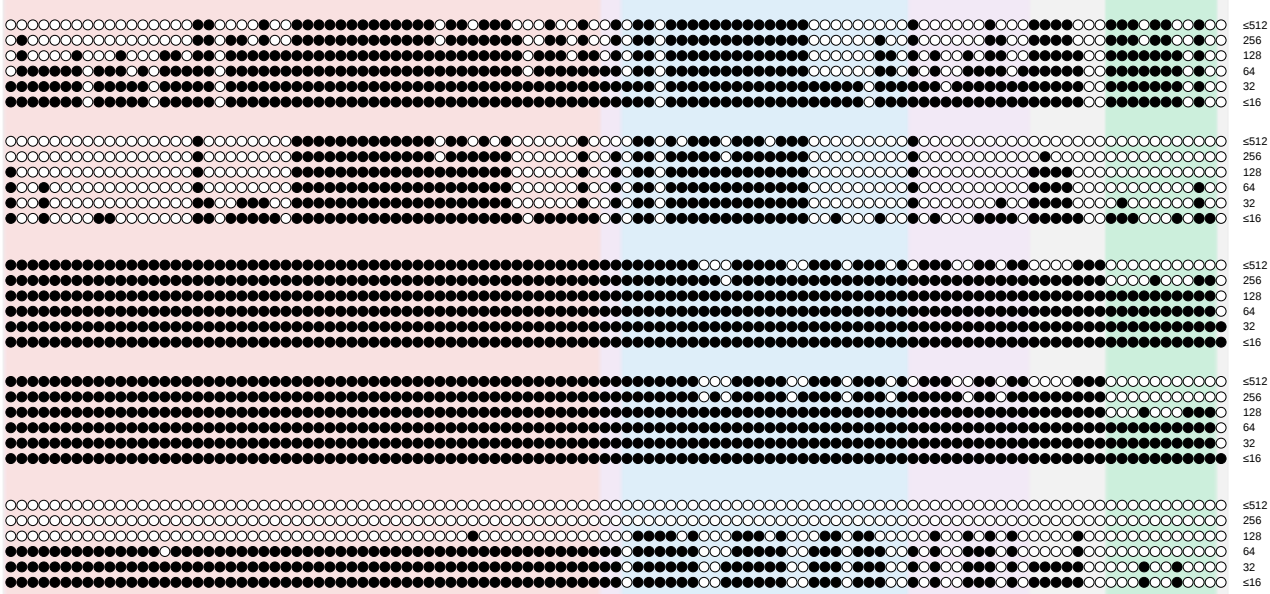
C

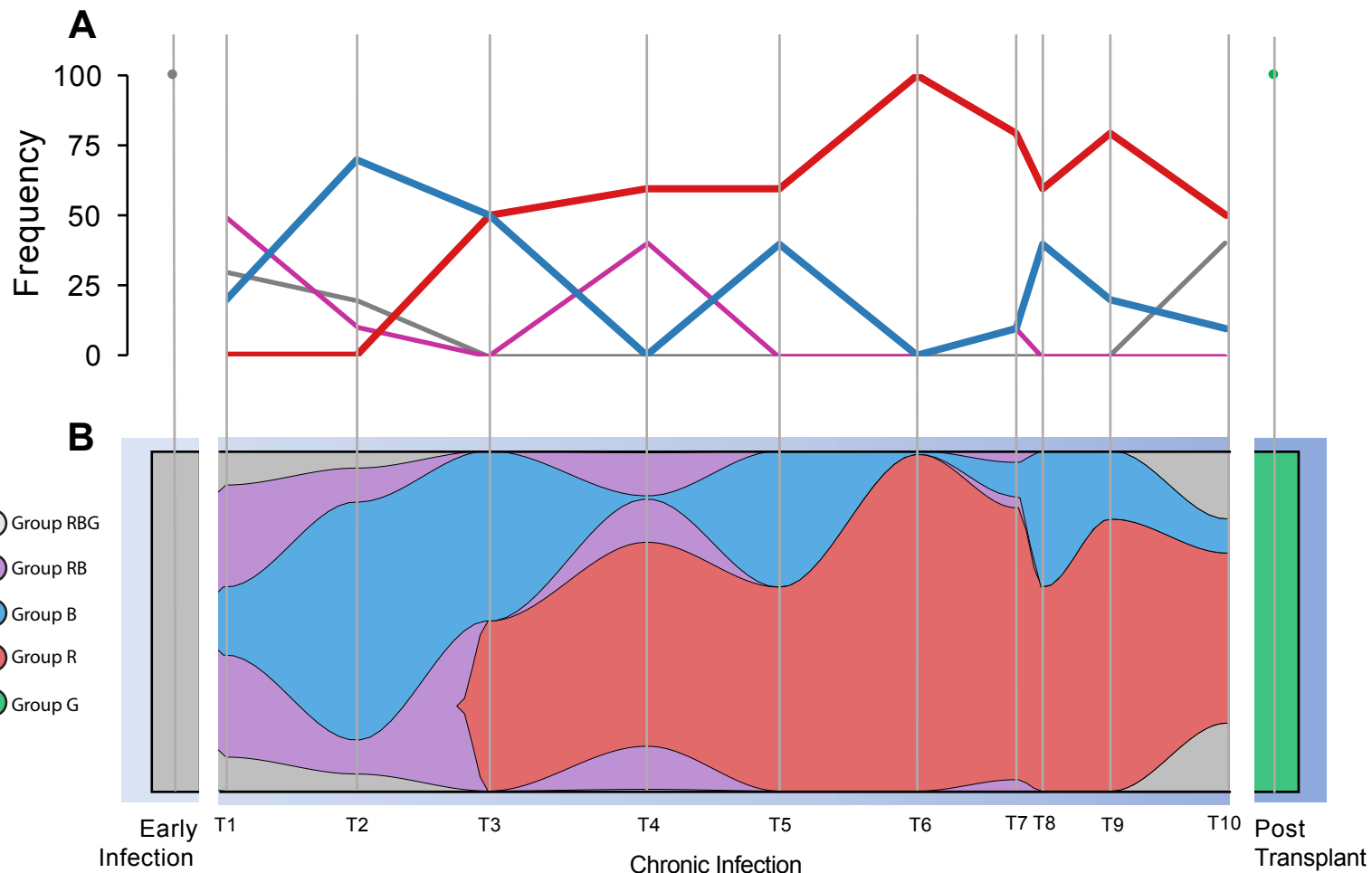


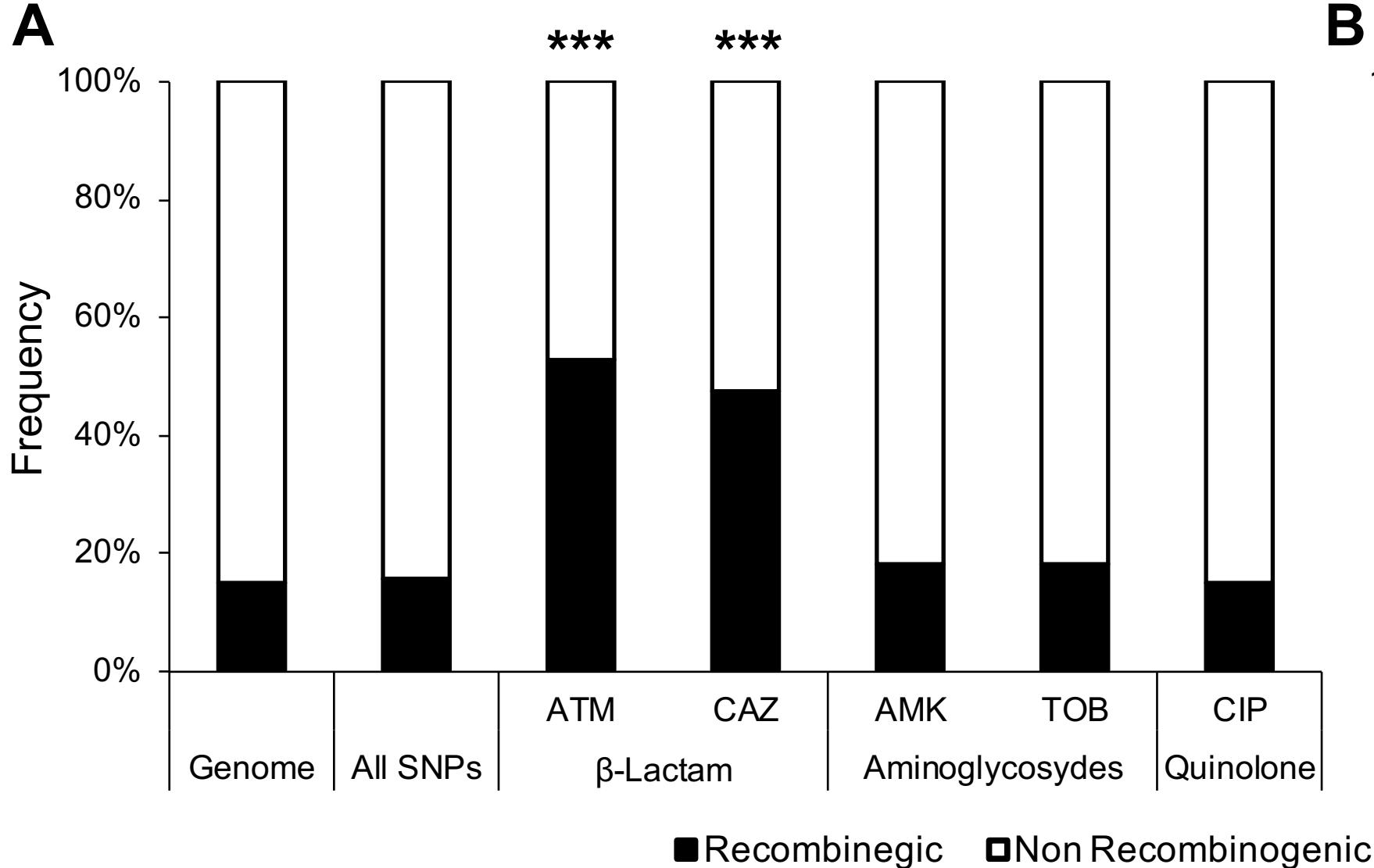
D



E





**A****B**